Photosynthesis Research (2019) 141:99–118
https://doi.org/10.1007/s11120-018-0601-1

ORIGINAL ARTICLE

A generalised dynamic model of leaf-level C_3 photosynthesis combining light and dark reactions with stomatal behaviour

Chandra Bellasio[1,2,3]

Received: 16 March 2018 / Accepted: 27 October 2018 / Published online: 23 November 2018

Abstract

Global food demand is rising, impelling us to develop strategies for improving the efficiency of photosynthesis. Classical photosynthesis models based on steady-state assumptions are inherently unsuitable for assessing biochemical and stomatal responses to rapid variations in environmental drivers. To identify strategies to increase photosynthetic efficiency, we need models that account for the timing of CO_2 assimilation responses to dynamic environmental stimuli. Herein, I present a dynamic process-based photosynthetic model for C_3 leaves. The model incorporates both light and dark reactions, coupled with a hydro-mechanical model of stomatal behaviour. The model achieved a stable and realistic rate of light-saturated CO_2 assimilation and stomatal conductance. Additionally, it replicated complete typical assimilatory response curves (stepwise change in CO_2 and light intensity at different oxygen levels) featuring both short lag times and full photosynthetic acclimation. The model also successfully replicated transient responses to changes in light intensity (light flecks), CO_2 concentration, and atmospheric oxygen concentration. This dynamic model is suitable for detailed ecophysiological studies and has potential for superseding the long-dominant steady-state approach to photosynthesis modelling. The model runs as a stand-alone workbook in Microsoft® Excel® and is freely available to download along with a video tutorial.

Keywords Mechanistic model · Microsoft® Excel® · Stomatal model · Time · Transients · Stomatal conductance · Assimilation · Photorespiration · Light fleck

Introduction

The pace of increases in crop yields has stalled over recent decades, urging researchers to develop innovative solutions to safeguard the productivity necessary to sustain expected future global demand for food and feed (Ray et al. 2012, 2013). The photosynthetic efficiency of C_3 crop plants falls short of theoretical potentials and is little or negatively affected by selective breeding (Long et al. 2015), making efficiency gains a key aim for improving yields from existing agricultural land (Taylor and Long 2017). Photosynthetic responses to dynamic environmental drivers are increasingly recognised as an area where photosynthetic efficiency can be improved by minimising the assimilatory and, or stomatal lag response(s) to environmental fluctuations, particularly light intensity (Kaiser et al. 2014; Lawson and Blatt 2014).

Leaves may experience large transient variations in light intensity [measured as photosynthetic photon flux density (PPFD)] as they move into the shade of leaves higher in the canopy and clouds move overhead to create light- and shade-flecks of varying intensity and spectral quality (Bellasio and Griffiths 2014; Pearcy et al. 1985; Pearcy 1990; Valladares et al. 1997). Shaded leaves can contribute up to 50% of canopy photosynthesis (Long 1993; Long et al. 1996) and accurate quantification of CO_2 assimilation (A) requires modelling of leaf responses to fluctuations in the canopy light environment (Allen and Richardson 1968; Song et al. 2013). In addition, atmospheric CO_2 concentration (C_a) can vary locally under natural field conditions, but variability in

Electronic supplementary material The online version of this article (https://doi.org/10.1007/s11120-018-0601-1) contains supplementary material, which is available to authorized users.

✉ Chandra Bellasio
chandra.bellasio@anu.edu.au

[1] Research School of Biology, Australian National University, Acton, ACT 2601, Australia

[2] University of the Balearic Islands, 07122 Palma, Illes Balears, Spain

[3] Trees and Timber Institute, National Research Council of Italy, Sesto Fiorentino, 50019 Florence, Italy

C_a is more frequent and pronounced when [CO_2] is experimentally enriched (Hendrey et al. 1997).

Stomata and photosynthesis respond continuously to environmental changes, but stomatal adjustments, which regulate the diffusion of CO_2 into the leaf and the conductance of water vapour to the atmosphere (g_S), can be an order of magnitude slower than assimilatory responses (McAusland et al. 2016). This lack of coordination between carbon gains (A) and water losses (E) often results in suboptimal water-use efficiency (WUE = A/E) and photosynthetic shortfalls (Lawson and Blatt 2014; Bellasio et al. 2017). Further, A may be biochemically limited due to a lag time in the induction of biochemical activity following environmental fluctuations (Naumburg and Ellsworth 2002; Taylor and Long 2017). By improving the speed at which the photosynthetic machinery responds and adjusts to fluctuating environmental conditions, substantial accrual of marginal gains in A and water savings over time are possible (Bellasio et al. 2017; Lawson and Blatt 2014; McAusland et al. 2016; Way and Pearcy 2012).

Most photosynthesis models, used at leaf level and broader scales, are based on steady-state principles (for review Bellasio et al. 2016a, b). Assimilation is often predicted using steady-state submodels rooted in the Farquhar et al. (1980) framework, which have since been updated (Busch et al. 2017; Yin et al. 2014). Steady-state photosynthesis models tend to overestimate integrated A under fluctuating PPFD (Kaiser et al. 2014), but also under variable C_a (Hendrey et al. 1997). This results, for instance, in poor understanding of plant growth and acclimation responses in CO_2 enrichment experiments, particularly under free air CO_2 enrichment (FACE) conditions (Long et al. 2006). This confounds the interpretation of experimental findings and hinders prediction of vegetation responses to rising CO_2 levels in the future. Moreover, incorporation of the latest developments in plant manipulation, including the effect of a modified reductive pentose phosphate pathway (RPP, Driever et al. 2017) and light reaction processes (Kromdijk et al. 2016), require further biochemical complexity than that of traditional models. In broader scale vegetation modelling, photosynthesis models are coupled with models characterising stomatal behaviour (Berry et al. 2010; Beerling 2015; Bonan et al. 2014; Ostle et al. 2009; Sato et al. 2015). The stomatal submodels generally estimate g_S empirically from environmental or internal variables rather than from process-based mechanistic principles (Damour et al. 2010). Empirical models may lose accuracy as simulated conditions deviate further from those under which the models were calibrated (Way et al. 2011) and then cannot provide insight into underlying physiological mechanisms (Buckley 2017).

Dynamic models characterise photosynthesis and stomatal behaviour under non-steady-state conditions. Although dynamic models of photosynthesis and g_S exist (e.g. Kirschbaum et al. 1997; Laisk and Eichelmann 1989), their application has been limited by the accessibility of the code or because their treatment of photosynthetic processes is either phenomenological (Vialet-Chabrand et al. 2016; McAusland et al. 2016), elementary (Pearcy et al. 1997; Gross et al. 1991), or so complex as to require dedicated software and high-capability computing (Laisk et al. 2009; Wang et al. 2014a, b; Zhu et al. 2007, 2013). Consequently, most studies, including those simulating dynamic conditions, have used steady-state models (e.g. Taylor and Long 2017).

Here I developed a biochemical, process-based framework for modelling photosynthetic dark reactions that is incorporated with light reactions and coupled to a mechanistic hydro-mechanical model of stomatal behaviour. I demonstrate its applicability using a range of examples including classical A–PPFD and A–C_i response curves, a mid-term acclimation to variable C_a and PPFD, and response to rapid transitions in light intensity and oxygen concentration. To maximise the potential user base of the model, I coded and developed it in a Microsoft® Excel® workbook, which is openly available from the Supplementary Information along with a video user guide (https://youtu.be/OVnxdn2G2rE).

Model development

Overview

A process-based, stock-and-flow model of leaf-level C_3 photosynthesis that runs in Excel® was developed incorporating leaf-level diffusion with a comprehensive treatment of assimilatory biochemistry and stomatal behaviour (Fig. 1, equations are detailed in Appendix). The modelled leaf consists of three compartments: the atmosphere, intercellular space and mesophyll. The processes of CO_2 diffusion through stomata, and CO_2 dissolution and hydration are described mechanistically. To reduce computational requirements, intercellular space and mesophyll are assumed uniform with no internal concentration gradients. Consequently, limitations imposed by the diffusion of metabolites are not considered. This is justified by a number of studies showing minimal reduction in A by heterogeneous distribution of metabolites (Wang et al. 2017; Retta et al. 2016; Tholen et al. 2012; Ho et al. 2015).

A light reactions submodel, modified from Yin et al. (2004), was used to estimate the potential rates of ATP and NADPH production for any PPFD. In the original Yin et al. (2004) formulation, the ratio of ATP to NADPH production rates could be adjusted by varying the cyclic electron flow rate (CEF, although this is close to zero for C_3 types). However, up-regulating CEF required additional light to be absorbed by photosystem I (PSI) because a constant electron

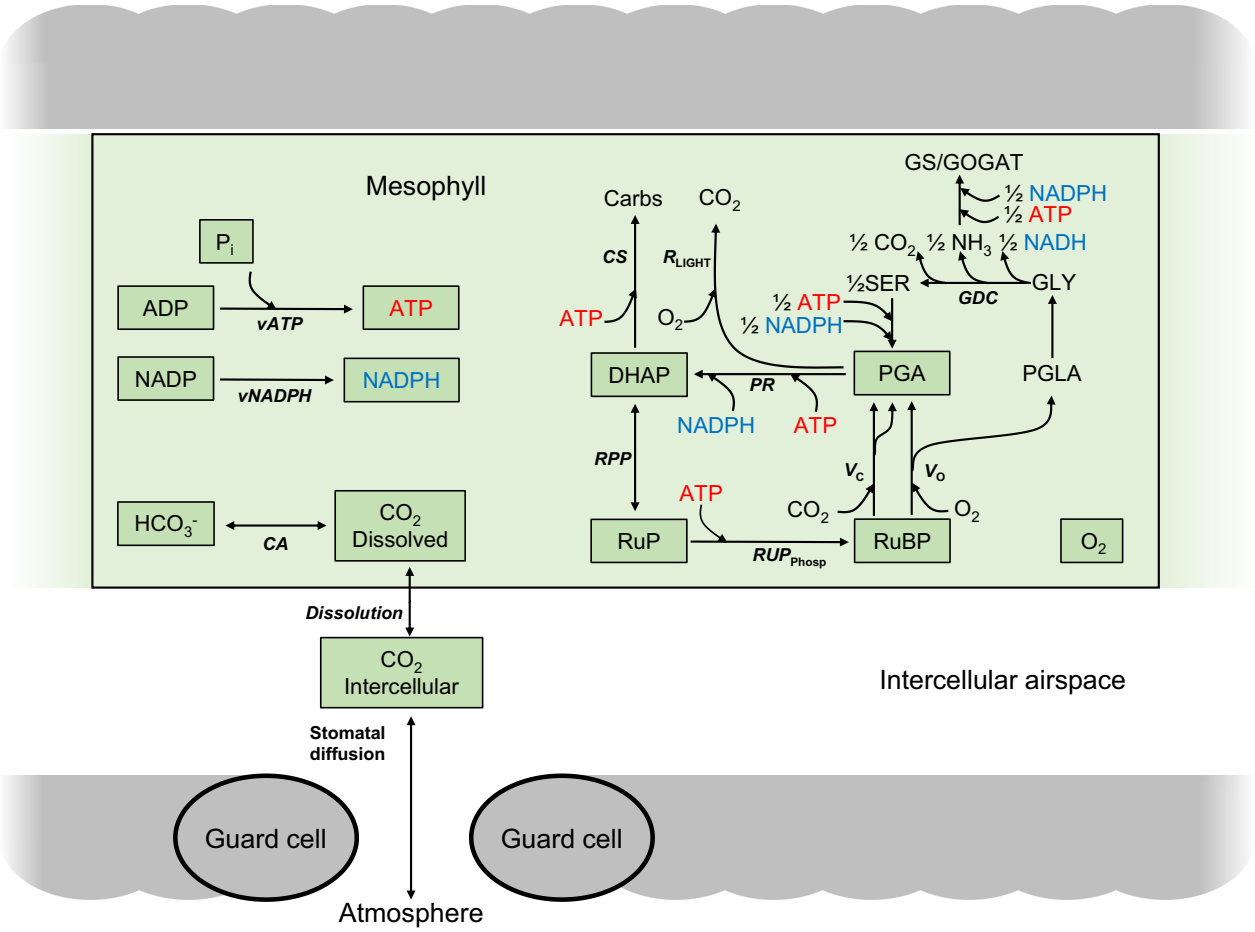

Fig. 1 Schematic model. The leaf is represented by three uniform compartments: the external atmosphere, the mesophyll and the intercellular space. The intercellular space communicates with the surroundings through stomata, which regulate CO_2 diffusion and respond to biochemical and hydro-mechanical forcing. Intercellular CO_2 dissolves, reaching a mesophyll CO_2 pool (all pools are represented by boxes) and may undergo enzymatic hydration. Rubisco carboxylation (V_C, with two arrows to symbolise the production of two PGA molecules) and oxygenation (V_O) reactions consume RuBP and produce PGA and PGLA. PGLA is recycled through the photorespiration cycle eventually regenerating PGA (concentrations of intermediate metabolites are not calculated). PGA is the substrate for respiration (R_{LIGHT}) and is reduced (PR) to triose phosphate (DHAP), which is the substrate of carbohydrate synthesis (CS). In this model, carbohydrates—the final product of photosynthesis—are generic triose that vanishes once synthesised. The majority of DHAP enters the sugar conversion phase of the RPP cycle, which is simulated as a single reversible step. Light reactions (depicted in the top left-hand side) supply the ATP and NADPH pools. The concentration of O_2 is assumed to equal the ambient concentration

flow through PSII (J_2) was assumed to facilitate implementation with fluorescence measurements. Here, a constant level of total light absorbed by PSI and PSII was used and was partitioned between photosystems using Yin et al. (2004) equations but modified (see Fig. 2) to account for the presence of the nicotinamide adenine dinucleotide (NADH) dehydrogenase-like (NDH) complex (Ishikawa et al. 2016; Yamori and Shikanai 2016).

After passing through PSI, electrons are either cycled to plastoquinone, used by alternative sinks ($J_{Pseudocyc}$ includes all sinks that are not assimilatory dark reactions, such as O_2 and NO_3^-), or used to reduce $NADP^+$ (J_{NADPH} is the NADPH used in assimilatory dark reactions). In this way, the power requirements for nitrogen reduction (Busch et al. 2017) are explicitly accounted for as a fraction of pseudocyclic electron flow ($f_{Pseudocyc\ NR}$), in line with Yin and Struik (2012). The remainder is consumed by the water–water cycle, also modelled explicitly. Although $f_{Pseudocyc}$ has a small value [~0.1, (Yin et al. 2004; Yin and Struik 2012)], its inclusion is important, as it influences the ATP/NADP ratio. The total ATP production rate (J_{ATP}) was obtained by summing the proton flow to the lumen and dividing by h, the number of protons required by ATP synthase. The potential rates of ATP and NADPH production are used by ATP and NADPH synthesis, which were modelled through a Michaelis–Menten kinetics function after Wang et al. (2014a). The proportion of actual to potential ATP and NADPH synthesis continuously feeds back to dark reactions by adjusting

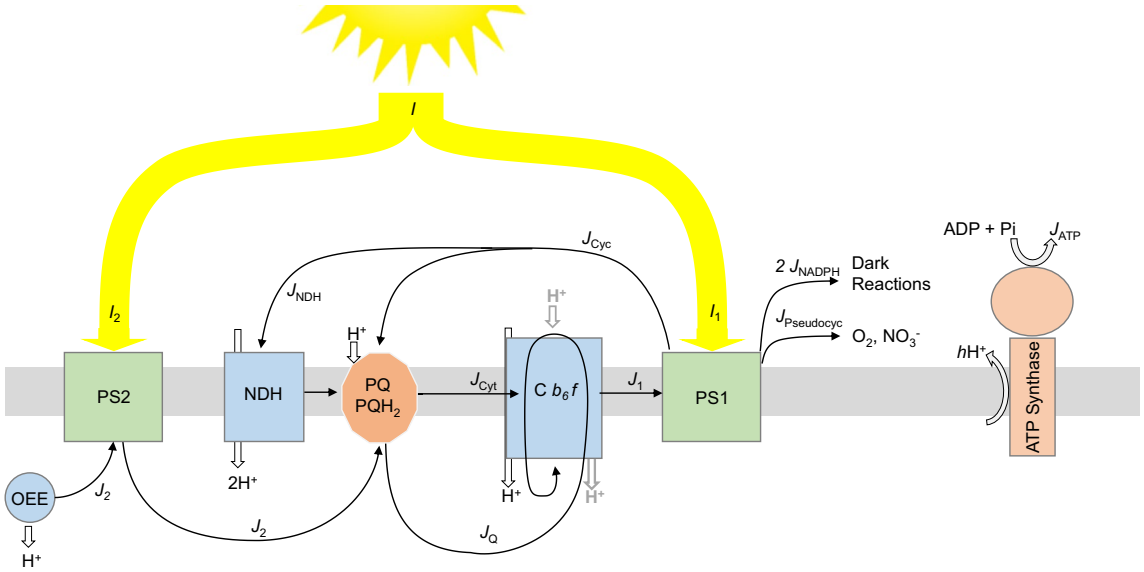

Fig. 2 Schematic of the light reactions submodel. Light is shown in solid yellow, electron fluxes in black, protein complexes are drawn as boxes, and proton delivery to the lumen is depicted by block arrows. A fraction of the light incident on the leaf (PPFD), I, is absorbed by PSI (I_1) or PSII (I_2). Electrons flowing through PSII (J_2) reach the plastoquinone and plastoquinol pool (PQ and PQH_2), simultaneously taking up protons from the stroma. Electrons flow to the Cytochromes b_6f where they may undergo so-called Q-cycling, which results in the translocation of one additional proton (shown in grey), eventually reaching PSI through plastocyanin (not shown). Here, electrons may either be cycled back through CEF (J_{Cyc}) to PQ; be used for alternative sinks (these include O_2 and NO_3 in this model); or be used by photosynthetic dark reactions. CEF can also follow two different paths, either the PGR5-mediated CEF or through the NDH complex, which translocates two additional protons across the thylakoid membrane. ATP synthase regenerates one molecule of ATP for each h proton returned to the stroma

PSII yield [Y(II)] and the level of CEF. Time delay functions allow simulation of photosynthetic acclimation of the potential rate of ATP (J_{ATP}) and NADPH (J_{NADPH}) synthesis to changes in PPFD.

A dynamic submodel of dark reactions, including key reactions involved in the RPP cycle, photorespiration pathway and carbohydrate synthesis (CS), was developed by synthesis of the model of Zhu et al. (2007). This model related enzyme activity to the concentration of substrates, including ATP and NADPH, and enzyme kinetic properties. Equations were simplified where possible with modifications according to the theoretical work of Bellasio (2017). Metabolite flows were calculated using a set of differential equations derived from the stoichiometry of Bellasio (2017) by removing the assumption of steady state. Time delay functions are used for Rubisco activation state (R_{act}) and CS.

The model also includes a stomatal component based on the hydro-mechanical formulation of Bellasio et al. (2017), developed after Buckley et al. (2003) and Rodriguez-Dominguez et al. (2016). Hydro-mechanical forcing links guard cell responses to leaf water status and turgor, which are in turn related to soil water status and plant hydraulic conductance. Leaf turgor varies from a maximum value (corresponding to negative osmotic potential, π_e) to zero as a function of the equilibrium between water demand (determined by the leaf-to-boundary layer water mole fraction gradient [D_S] and g_S) and water supply (determined by soil water potential, Ψ_{Soil}, and soil-to-leaf hydraulic conductance [K_h]). The influence of biochemical factors relative to hydro-mechanical forcing is determined by the parameter β (defined as hydro-mechanical/biochemical response parameter), while stomatal morphology is described by χ (defined as turgor-to-conductance scaling factor). The strength of biochemical forcing (accounting for factors such as light intensity and CO_2 concentration) is represented by τ. In this formulation, τ was set to equal f(RuBP), a function describing the degree of ribulose 1,5-bisphosphate (RuBP) saturation of RuBP carboxylase/oxygenase (Rubisco) active sites; thus, τ is a measure of the balance between the light and dark reactions of photosynthesis, *in sensu* Farquhar and Wong (1984). Consistent behaviour of τ is supported via evidence suggesting that stomata respond to the supply and demand for energy carriers in photosynthesis (Wong 1979; Busch 2014; Mott et al. 2014; Messinger et al. 2006)—i.e. increasing with PPFD and decreasing with C_i. The use of τ as a predictor of stomatal behaviour is empirically based. This is justified by its capacity to predict parallel events occurring in chloroplasts and guard cells, but I make no claim about whether τ offers a faithful mechanistic description of stomatal behaviour (for discussions see Farquhar and Wong 1984; Bellasio et al. 2017; Buckley 2017).

Stomata respond to any perturbation with a delay due to the kinetics of adjustment of guard cell osmotic pressure. The time constant for that delay is species specific and typically differs between opening and closing movements (Lawson and Blatt 2014). With the delay functions included, the stomatal submodel can be used for simulating the g_S dynamic response to fast changes in humidity, hydraulic conductance and Ψ_{Soil} (but see considerations on the 'wrong way response' made in Bellasio et al. 2017). Yet, because changes in these inputs typically occur on timescales of hours to weeks, they will be approximated by steady-state behaviour, not addressed here (but see Bellasio et al. 2017). The model should also be suitable for calculating fast dynamics of g_S in response to light flecks (e.g. Pearcy et al. 1997), though g_S responses shorter than 1 min have not yet been calibrated.

Parameterisation

Literature values for the different parameters were averaged because the aim was to simulate realistic, general behaviour, not behaviour specific to a particular species or environmental conditions. Values for the parameters are reported in Supplementary Tables S1 and S2. Biochemical constants were primarily derived from Zhu et al. (2007) and Wang et al. (2014a, b). Some biochemical and electron transport parameters were taken from Bellasio et al. (2016b), or from von Caemmerer (2000). Stomatal parameters were taken from, or assigned values similar to, Bellasio et al. (2017). For parameterisation of combined or simplified processes, I either derived parameters from the original equations or assigned plausible, physiologically realistic values. Parameters defining the PPFD dependence of Rubisco activation (Eq. 19) were initially set at values from Seemann et al. (1988) and adjusted by fitting the steady-state PGA concentration in light curves shown in Fig. 4. Parameters defining the dependence of Rubisco activation on CO_2 concentration at the M carboxylating sites, C_M (Eq. 20) were derived empirically following these considerations: (1) by comparing measurements and model outputs (Figs. 3, 4) and considering data from Sage et al. (2002) I established that Rubisco is fully activated for C_M above 200 µmol mol^{-1}; (2) tangible inactivation occurs for C_M below 100 µmol mol^{-1} (Sage et al. 2002); and (3) activity decreases to zero for [CO_2] approaching zero (Portis et al. 1986), but yet a substantial residual activity exists for CO_2 concentration around the CO_2 compensation point. The values were then adjusted by fitting the steady-state PGA concentration in A/C_i curves shown in Fig. 4, and the final values proposed are shown in Table S2. Additional parameter tuning may be required before the model is applied to specific species or growth conditions.

Outputs

At each time step, the model calculates nine metabolite stocks (expressed both as mol per metre square of leaf or concentration, mM): C_i, mesophyll [CO_2], bicarbonate, RuBP, PGA, dihydroxyacetone phosphate (DHAP), ATP, NADPH and ribulose 5-phosphate (Ru5P). The concentrations of inorganic phosphorus (P_i), adenosine diphosphate (ADP) and NADP are calculated by subtraction from a total pool (Fig. 1). From this, 12 flow rates are calculated (expressed in mmol m^{-2} s^{-1} and plotted in the figures in units of µmol m^{-2} s^{-1}): actual ATP and NADPH synthesis (v_{ATP} and v_{NADPH}), Rubisco carboxylation and oxygenation (V_C, and V_O), rates of glycine decarboxylase (GDC), phosphoribulokinase (RuP_{Phosp}), PGA reduction (PR), CS, CO_2 stomatal diffusion, CO_2 dissolution, carbonic anhydrase hydration (CA), and the reactions through the RPP cycle.

Simulations

A typical dynamic simulation involves first clearing any previous results, defining the initial state of the leaf, including metabolite concentrations (see Supplementary Table S2), and then iteratively calculating the 'flows' and subsequent variation in 'stocks'. Over time, the stocks reach steady state, where they depend solely on flows, but not on their initial value. A dynamic simulation may involve perturbing steady-state conditions, and observing how a new steady state is reached. Figure S1 shows a typical trace of an output quantity (CO_2 stomatal diffusion) plotted over time, while C_a and PPDF were varied to simulate a typical gas exchange experiment.

A–PPFD and *A*–C_i response curves

Figure 3 shows the modelled response of A, g_S and v_{NADPH} to variation in PPFD and C_a. Model output corresponding to the values calculated for the last second of each PPFD or C_a step is compared with Bellasio et al. (2016b) A–PPFD and A–C_i response curves measured in tobacco. Overall, the agreement between observations and model output was high, even if the model was parameterised with literature values not explicitly fitted to the data. For the A–PPFD curves, there was no noteworthy deviation between modelled and observed values of A, g_S or v_{NADPH} (Fig. 3, left-hand panels). There was also overall good agreement between modelled and measured A–C_i curves, though both A (Fig. 3b) and v_{NADPH} (Fig. 3f) were underestimated at ambient O_2 and $C_i > 300$ µmol mol^{-1}, and g_S was slightly overestimated at low C_a (Fig. 3d). Further analysis revealed that under these conditions, modelled A was relatively unresponsive to individual increases in relevant flow rates including J_{ATP} and

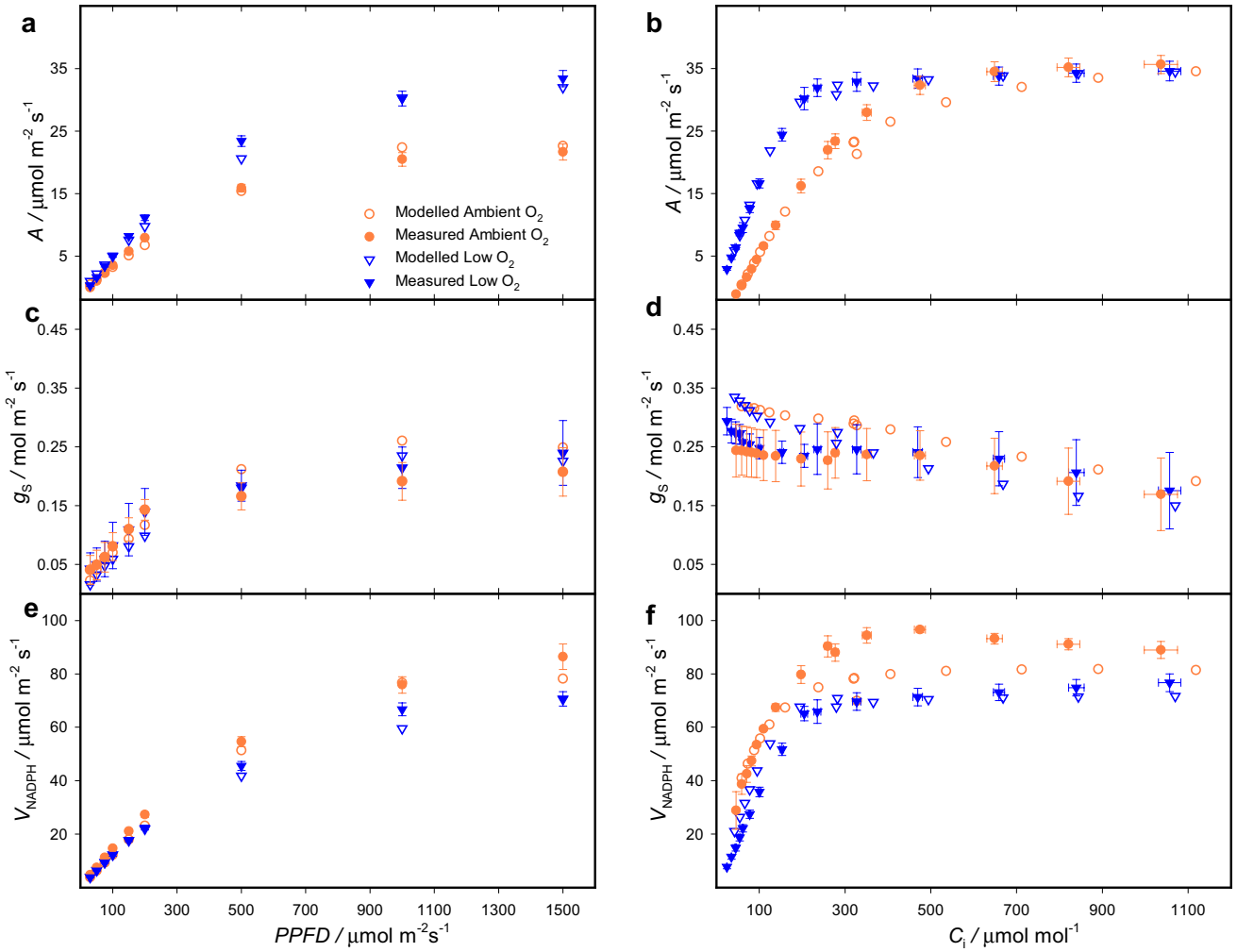

Fig. 3 Simulated A–C_i and A–PPFD response curves. Gas exchange experiments simulated with time increments of 1.5 ms. Modelled responses of assimilation rate, A (**a, b**), stomatal conductance, g_S (**c, d**), and NADPH production rate, v_{NADPH} (**e, f**) to incident irradiance, PPFD (left) and $[CO_2]$ in the intercellular space, C_i (right) at 21% O_2 (open circles) and at 2% O_2 (open triangles). The model is plotted against data from Bellasio et al. (2016b) measured under 21% O_2 (closed circles) and at 2% O_2 (filled triangles). Error bars show ± 1 SE. Details of parameterisation are given in Supporting Tables S1 and S2

J_{NADPH} synthesis, RuP phosphorylation and V_C. This suggests complex, concurrent regulation of light and dark reactions that require further exploration.

Steady-state concentration of photosynthetic metabolites

Figure 4 compares model output for different metabolite pools with data measured by von Caemmerer and Edmondson (1986) on radish leaves. In that experiment, photosynthesis was allowed to reach full induction before measurements were taken; therefore, 1800 s were allowed between each model step to ensure *quasi* steady state. RuBP concentration was underestimated in the A–PPFD curve (Fig. 4a), but correctly estimated it in the A–C_i curve at ambient CO_2 concentration (Fig. 4b), suggesting that the model properly averaged data. At 2% O_2, the model replicated the measured RuBP concentration at low C_i, but it underestimated it at high C_i (Fig. 4b). The variation in PGA concentration as a function of C_i, both under low and ambient O_2 (Fig. 4d), was well captured by the model. However, the PGA pool was overestimated when PPFD < 500 µmol m^{-2} s^{-1} (Fig. 4c).

The model also captured the overall trends in relative Rubisco activity in response to PPFD and C_i at different O_2 concentrations, though absolute values were underestimated (Fig. 4e, f). At low C_i, Rubisco deactivation is due to the decarbamylation of the active site, captured by $f([CO_2])$. At low PPFD, the decrease in Rubisco activity is due to the redox regulation of Rubisco activase, captured by f(PPFD). The model calculates the relative activity of Rubisco as the product of f(RuBP) and Rubisco activation state (R_{act}). In contrast, measured data come from comparing the in vitro Rubisco activity under physiological conditions with the

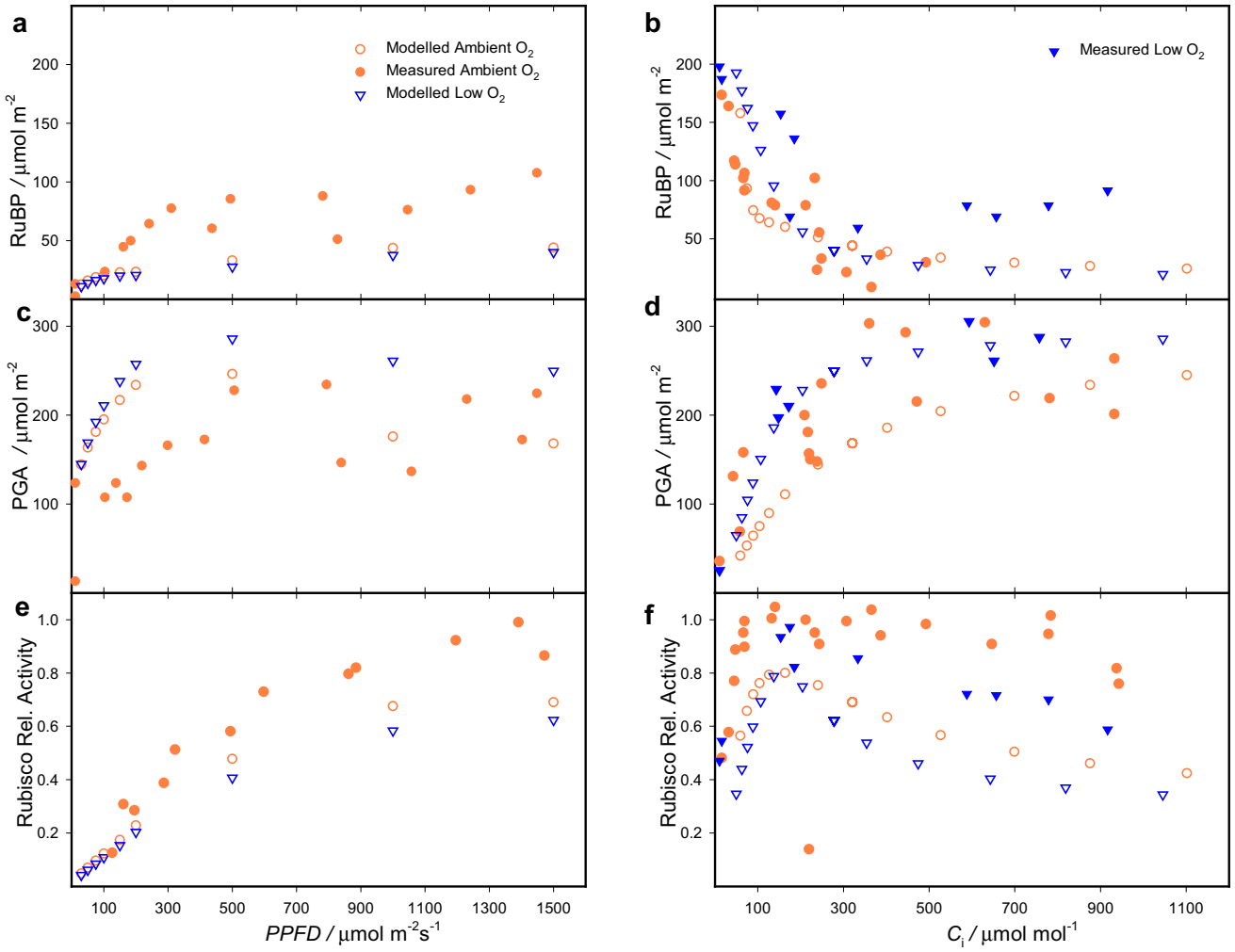

Fig. 4 Metabolite concentrations at steady state. The model was run for 1800 s at different levels of PPFD (left-hand panels) or C_a (right-hand panels) until quasi steady state was reached. Panels **a, b** RuBP concentration; Panels **c, d** PGA concentration; Panels **d, e** relative Rubisco activity calculated as $f(\text{RuBP}) \times R_{act}$. The model (open symbols) is plotted against data from von Caemmerer and Edmondson (1986) (closed symbols) measured under 21% O_2 (circles) and at 2% O_2 (triangles). Parameterisation was maintained from previous simulation, see Supporting Tables S1 and S2

in vitro activity of Rubisco after full induction of enzymatic activity. The discrepancy between model and observed absolute values is plausible because the modelled activity also accounts for the effect of partial RuBP saturation, while in vitro data were taken under full RuBP saturation.

At steady state, under a PPFD of 500 µmol m^{-2} s^{-1}, the ratio [DHAP]/[PGA] was 0.2 between the values of 0.1 (in the stroma) and 0.35 (in the cytosol) measured in the light (400 µmol m^{-2} s^{-1}) by Heineke et al. (1991). Modelled values for the ratio [ATP]/[ADP] under a PPFD of 500 or 1000 µmol m^{-2} s^{-1} were ~ 1.5 and 7, respectively, which compare well with the ratio of 3 measured in the light by Heineke et al. (1991). Finally, the model predicted a [NADPH]/[NADP] ratio of 0.16 and 0.5 under the PPFD of 50 and 1000 µmol m^{-2} s^{-1}, respectively, that is similar to the values of 0.2 and 0.5 measured by Heineke et al. (1991) for dark and light conditions, respectively.

Notably, this output was obtained with identical parameterisation to the previous simulations with tobacco.

Dynamic responses to an increase and decrease in PPFD

A simulation were run to replicate the response of a spinach leaf to a steep increase and decrease in PPFD at 21% O_2 (unpublished data courtesy of Ross Deans, Farquhar Lab, Australian National University). The leaf was acclimated under a PPFD of 50 µmol m^{-2} s^{-1} until steady state was reached, and subsequently PPFD was increased to 1500 µmol m^{-2} s^{-1}. Model parametrisation was the same as in preceding simulations with tobacco and radish, except for maximum rate of Rubisco carboxylation ($V_{C\,MAX}$) and the

speed of stomatal opening. Simulated dynamic responses of A and g_S corresponded closely with the measured data (Fig. 5a, c). After the steep increase in PPFD, ATP and NADPH production rates (Fig. 5a), the Rubisco activation state (Fig. 5b), and ATP and DHAP concentrations (plotted as relative to the total pool of adenylates in Fig. 5g) followed a hyperbolic increase. ATP production increased faster than Rubisco activation state, which resulted in an initial decrease

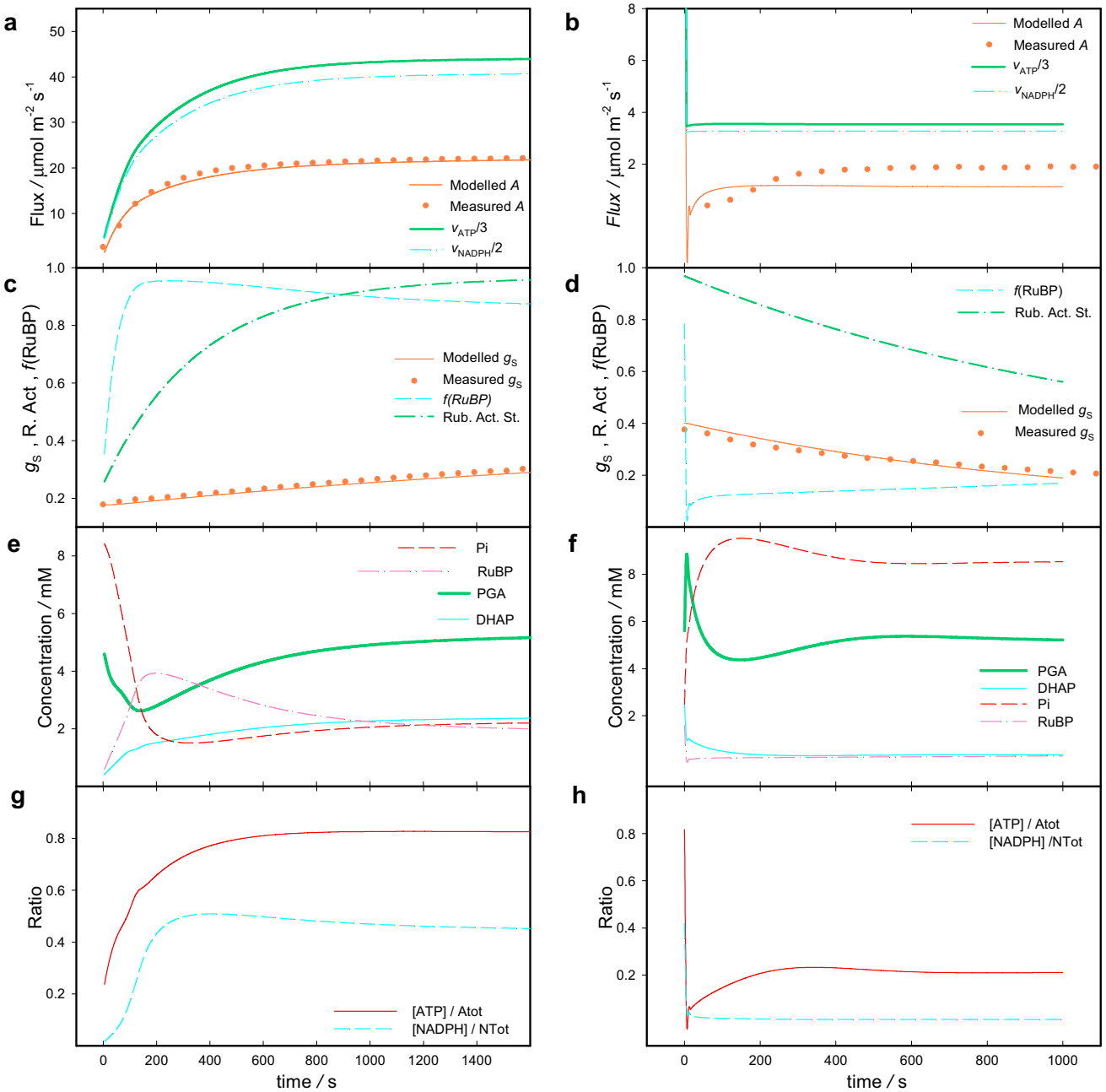

Fig. 5 Response to a transition from low to high light and from high to low light. Circles show the average of $n=3$ measurements taken on spinach (*Spinacia oleracea*, courtesy of Ross Deans, unpublished). The leaf was acclimated under a PPFD of 50 µmol m^{-2} s^{-1} (left) or 1500 µmol m^{-2} s^{-1} (right) until steady state was reached, then PPFD was increased to 1500 µmol m^{-2} s^{-1} or decreased to 50 µmol m^{-2} s^{-1} and the variation in leaf-level assimilation, A (**a, b**), stomatal conductance, g_S (**c, d**) and CO_2 concentration in the intercellular space, were recorded every 10 s. Lines show model outputs: rate of ATP and NADPH synthesis, and A (panels **a, b**); g_S, f(RuBP) and Rubisco activation state (**c, d**); concentrations of metabolites (**e, f**); ATP and NADPH concentrations (**g, h**). For simulations, C_a was the same as in the measurement cuvette (350 µmol mol^{-1}), $V_{C\,MAX}=0.18$ mmol m^{-2} s^{-1}, stomatal characteristics were adjusted at $\chi\beta=0.8$ mol air MPa^{-1}, $\tau_0=-0.12$, $K_i=3600$ s; $K_d=1200$ s all other parameters were maintained from previous simulations (Supporting Tables S1 and S2)

in [PGA], a fast increase in [RuBP] and a subsequently sharp decrease in [P_i] (Fig. 5e). After ~ 150 s, there was a continuous smooth decrease in f(RuBP), resulting from the combination of increasing [PGA] and decreasing [RuBP] (Fig. 5c).

Decreasing PPFD from 1500 µmol m^{-2} s^{-1} to 50 µmol m^{-2} s^{-1} resulted in a sharp initial reduction in modelled A, followed by a hyperbolic increase to a new steady-state value (Fig. 5b). The steady state modelled A slightly underestimated the measured rate (Fig. 5b). A similar pattern was followed by f(RuBP) (Fig. 5 d) and [ATP] (Fig. 5h), although they reached steady state faster and slower than A, respectively. The ATP and NADPH production rates (Fig. 5b) and [NADPH] (Fig. 5h) reached steady state almost immediately after an initial spike. The model closely resembled the measured slow decrease in g_S (Fig. 5d). The response of Rubisco activation state (Fig. 5d) was similar, although faster, than the observed trend in g_S. [PGA] sharply increased in the initial seconds after light reduction and then decreased to a new steady-state value where [P_i] was higher than the initial value at high PPDF (Fig. 5f). The initial sharp increase in [PGA] was possible due to a high Rubisco activation state. This depleted the pool of RuBP, which could not be regenerated because of insufficient light. The trend in [DHAP] was comparable to the simulations of Laisk et al. (1989) [Fig. 11 in Laisk et al. (1989)]. In contrast to this model, Laisk et al. (1989) model predicted that [ATP], [P_i] and intermediates of the RPP cycle had smooth transitions to steady state after perturbation without local maxima or minima. My simulations are perhaps more realistic as they resemble measurements of [P_i] and [ATP] by Santarius and Heber (1965), although with slower kinetics.

Dynamic responses to an increase and decrease in C_a

Model predictions for a steep increase (from 350 to 1500 µmol mol^{-1}) or decrease (from 1500 to 350 µmol mol^{-1}) in C_a were compared with data by Laisk et al. (1991). CS was timed with a first-order exponential delay function analogous to Eq. 41 with a time constant of 35 s. After the sudden increase in C_a, A increased above 40 µmol m^{-2} s^{-1} for ~ 1 s, which I attribute to the dissolution of CO_2 into the leaf, then stabilised ~ 36 µmol m^{-2} s^{-1} for ~ 30 s, which I attribute to the carboxylation of the pool of phosphorylated metabolites. Finally A reached a minimum (Fig. 6a) coincident with a minimum in [P_i] (Fig. 6e), v_{ATP} (Fig. 6a) and [ATP] (Fig. 6g). After these three phases, all modelled quantities approached steady state smoothly.

After a steep decrease in C_a (Fig. 6 b, d, f, g), A decreased for ~ 1 s below the steady-state value before the perturbation, which can be explained by the stripping of dissolved CO_2 out of the leaf. Subsequently A smoothly approached a new steady-state value. The [PGA] reached a minimum after ~ 80 s, which determined a maximum in [P_i] and a consequent maximum in v_{ATP} and [ATP].

Overall, the model captured the dependence of A on P_i dynamics, which underpins the so-called photosynthetic oscillations (Walker 1992). Further, modelled v_{ATP} (which is a function of the reciprocal of leaf fluorescence) replicated the pattern of fluorescence shown by the simulations of Laisk and Eichelmann (1989) [their Fig. 5]. However, neither the model of Laisk and Eichelmann (1989) nor mine captured the measured response of A beyond 30 s of induction, consisting of a very deep trough in A lasting 10–20 s, followed by 4–5 dampened oscillations with a period of ~ 60 s leading to a new steady state.

Dynamic responses to a decrease in atmospheric O_2 concentration

A simulation was run to replicate the experiment of Bellasio et al. (2014), which involved assessing the response of A and Y(II) to a decrease in [O_2] in a tobacco leaf. The model accurately captured A and Y(II) at steady state before and after the reduction in [O_2]. The dynamic response of Y(II) was also closely reproduced (Fig. 7). However, modelled A failed to capture the initial spike measured in A immediately after the reduction in [O_2], which may be a measurement artefact that originated during adjustments of the infrared gas analyser.

Discussion

A newly derived process-based stock-and-flow biochemical model of photosynthesis was coupled to a dynamic hydro-mechanical model of stomatal behaviour. The new photosynthesis model features time-explicit constraints on J_{ATP}, g_S and Rubisco activation state. Steady-state metabolite concentrations are determined by environmental drivers and the kinetic parameters of enzymes, but not by initial metabolite concentrations. The coupled model achieved a stable and realistic rate of light-saturated A. After a perturbation in an environmental driver (e.g. PPFD), the model was able to regain a specific steady state. The model successfully replicated gas exchange experiments, including A–C_i and A–PPDF curves, and transient responses to steep changes in [O_2], C_a, and PPDF.

Simplifying assumptions

The mathematical description of dark reactions was simplified from Zhu et al. (2007) by reducing the number of metabolites and reactions simulated and removing some of the feedback loops. Offloading of the RPP cycle to photosynthetic sinks was simplified into a single process called

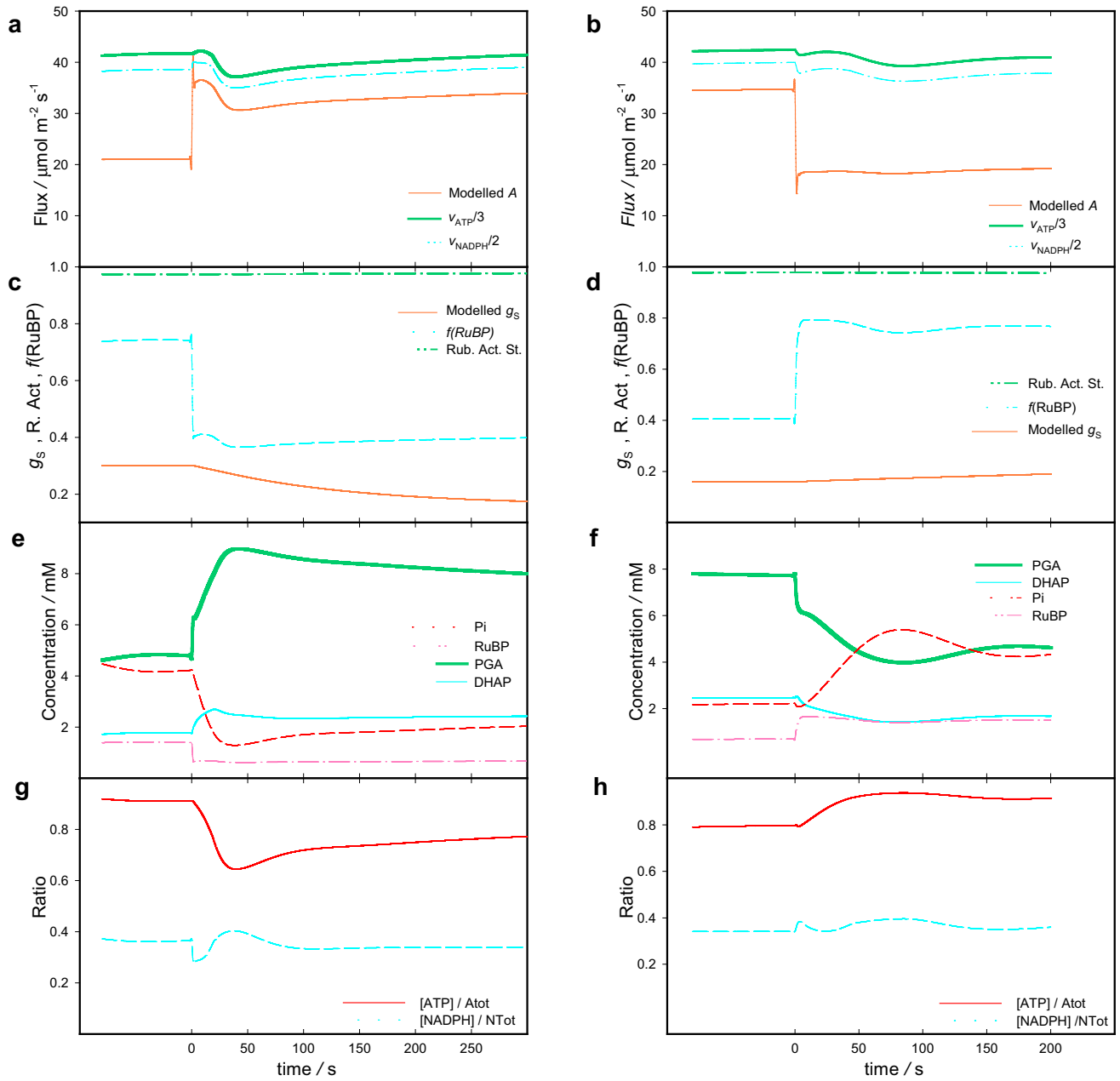

Fig. 6 Modelled response to a transition from ambient to high CO_2 and from high to ambient CO_2. The model was run at a C_a of 350 µmol mol^{-1} (left) or of 1500 µmol mol^{-1} (right) until steady state was reached. Then C_a was increased to 1500 µmol mol^{-1} or decreased to 350 µmol mol^{-1}. Lines show modelled rates of ATP and NADPH synthesis, and A (panels **a, b**); g_S, f(RuBP) and Rubisco activation state (**c, d**); concentrations of metabolites (**e, f**); ATP and NADPH concentrations (**g, h**). Parameters were the same as in Fig. 5

CS. Additionally, the reactions of the photorespiratory cycle were assumed non-limiting. Additional feedbacks from sedoheptulose-1,7-bisphosphatase (SBPase) and fructose-bisphosphate (FBP) (Wang et al. 2014b) were not included in the model. Feedbacks characterised in vivo involve redox regulation [e.g. Zhang and Portis (1999)]. However, in the model, the dynamics of PGA depend solely on the equilibrium between its formation by Rubisco and reduction. This approach was able to reproduce the response of PGA to PPDF observed by von Caemmerer and Edmondson (1986) (Fig. 4c). The pool of phosphorylated metabolites includes PGA, DHAP RuP and RuBP. Additional pools of sugar phosphates were added in pilot simulations, but for simplicity, were not included in the final model, nor was the activity of the malate shuttle (Foyer et al. 1992).

Dynamic simulation of electron transporters can be computationally demanding (Zaks et al. 2012); therefore, the flows associated with light reactions were described with

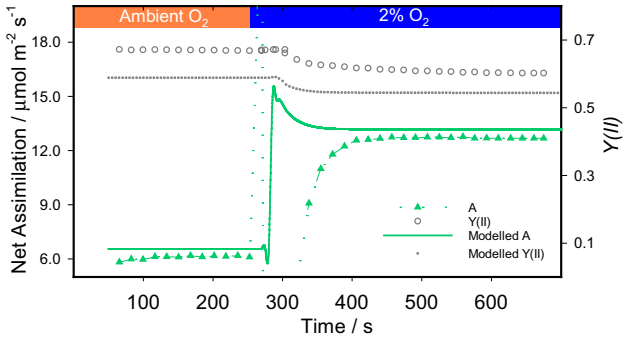

Fig. 7 Response to a transition from ambient to low atmospheric oxygen concentration. Open symbols show tobacco measurements from Bellasio et al. (2014) where the leaf was acclimated under a PPFD = 300 µmol m^{-2} s^{-1} and C_a = 200 µmol mol^{-1} until steady state was reached. Then the background gas was switched to 2% O_2 and the variation in leaf-level assimilation (*A*, triangles), and yield of photosystem II (*Y*(II), squares) were recorded every ~ 17 s. The model replicated this experiment. The solid line shows modelled leaf-level assimilation, while dots show modelled *Y*(II) calculated as $Y(\mathrm{II}) \approx \frac{V_{\mathrm{NADPH}}}{0.45 \times \mathrm{PPFD} \times s}$, where *s* is an energy conversion coefficient. In the model, C_a was set to equal C_a in the measurement cuvette, while all other parameters were maintained from Figs. 3 and 4 (Supporting Tables S1 and S2)

classical equations, in line with Wang et al. (2014a). This simplification implies that responses are instantaneous, which is physiologically plausible because the speed of light reactions is higher than that of dark reactions (Trinkunas et al. 1997). The model also ignored chloroplast movements, which have been shown to dynamically vary in some species (Davis et al. 2011; Morales et al. 2018). Respiration was assumed to be supplied by new assimilates [3-phosphoglyceric acid (PGA)] following the original formulation of Bellasio and Griffiths (2014) and subsequent developments (McQualter et al. 2016; Bellasio 2017). The ATP and NADH produced during respiration were neglected because they are likely to be consumed by basal metabolism. Although *CS* was made partially reversible (Eq. 28a), a calibration of metabolite replenishment in the dark is required before the model can be used for long simulations around or below light- or CO_2-compensation points. For further details on assumptions, see Bellasio et al. (2017) and Bellasio (2017).

Comparison with other models

The model presented here characterises biochemical processes more comprehensively than preceding models (Pearcy et al. 1997; Gross et al. 1991; Gross 1982) that featured phenomenological pseudoreactions (Morales et al. 2018) not mechanistically linked to enzyme activity. Additionally, my model is simpler, freely available, and therefore more readily applicable than earlier models (Wang et al. 2014b; Zhu et al. 2007, 2013; Laisk et al. 2009; Laisk and Edwards 2000, 2009; Laisk and Eichelmann 1989). Like the models of Wang et al. (2017) and Morales et al. (2018), my model also responds to PPFD and external CO_2 concentration, even at limiting levels. Importantly, in my model, light reactions can respond to transitions in atmospheric [O_2] (Fig. 6). In addition to linking Rubisco activation to PPFD (mediated by Rubisco activase), a feature that some other models encompass, a distinctive feature of my model is including a description of Rubisco inactivation at low [CO_2] (mediated by decarbamylation). I made both these drivers time dependent with empirical functions. Lastly, and uniquely, my model includes the process-based description of stomatal responses to a range of environmental drivers such as humidity and soil water availability.

There are two main differences between the dynamic photosynthesis model of Morales et al. (2018) and the model described here. In the model by Morales et al. (2018), there are two dynamic processes: Rubisco and a pseudoreaction associated to RuBP regeneration. In my model, there are nine dynamic reactions in the dark phase, which are mechanistically dependent on the concentration of 12 metabolites. In Morales et al. (2018), light reactions are simulated dynamically with explicit description of quenching phenomena. In my model, there is full integration between dark reactions and the electron transport chain, including: feedbacks at the level of CEF engagement; at the link between O_2 concentration and electron flow through the glutathione–ascorbate peroxidase (APX) cycle; and at the level of *Y*(II). The latter is dependent on [ATP], [NADPH] and [P_i] mediated by the kinetics of ATP synthesis.

In most dynamic and steady-state models, feedbacks are accounted for with a discontinuous function selecting between the 'minimum of' two or more quantities. For instance, Busch and Sage (2017) calculated *A* by selecting between three limiting factors: light, enzyme capacity, or triose phosphate availability. In Wang et al. (2014a) and preceding models, the calculation of V_C is underpinned by the selection between RuBP or CO_2 limitations. In my model, all biochemical feedbacks operate continuously. The transition from light- to enzyme-limitation is smooth, pivoting around the poise between regeneration and use of RuBP. This poise is captured by a quadratic function, *f*(RuBP), which depends on the concentration of RuBP relative to the concentration of Rubisco catalytic sites. This function was originally developed by Farquhar et al. (1980) (V_C/W_C in their notation, representing the actual, relative to the RuBP-saturated, rate of carboxylation), but it has rarely been implemented in its full quadratic form. The transition to TPU limitation is also smooth but in this case, is underpinned by a decreasing amount of P_i liberated by CS, thereby reducing [P_i] thats feedbacks directly on v_{ATP} and indirectly over *Y*(II). Under TPU limitation, assimilation is controlled by $V_{MAX\ CS}$.

Simulation processing time

On an ordinary desktop or laptop computer (~4 GB of RAM and ~2 GHz CPU speed), the model cycles at ~1000 Hz, with the actual time taken for a simulation run depending on the integration time step. The model is 'stiff'; therefore, the step length is constrained by stability requirements, rather than those of accuracy. The model becomes unstable when the fluxes accrued over the time step become comparable with the corresponding stocks. Of course, the fastest reactions such as those involving CO_2 diffusion and hydration are the most affected. If carbonic anhydrase (CA) is included in calculations, the model is unstable at time steps greater than 0.5 ms. Using an integration step of 0.3 ms, it takes ~35 s of computation time to simulate 10 s transition, and 42 h to simulate a 12-h photoperiod.

Stability can be improved by ignoring CA activity, which makes the model stable for time steps shorter than 2 ms. CA may be relevant at timescales shorter than 0.1 s and was included in the model because it has been deemed important in a number of recent studies (e.g. Ho et al. 2015); however, excluding CA did not change the model outputs presented here. Using a step of 1.5 ms, it takes ~7 s of processing time to simulate 10 s and 8.4 h to simulate a 12-h photoperiod.

Stability can also be ameliorated by incrementing the stocks. In this model, the residual leaf volume, occupied by cell walls and apoplastic solution, is all assumed to be intercellular air. A higher volume allows better model stability, because the flux of incoming CO_2 is buffered by a larger pool of air. Thickness and porosity may need to be adjusted for specific applications, for instance, for simulating airspace patterning manipulation (Lehmeier et al. 2017). Improvements in speed can also be achieved by assuming that CO_2 in the liquid phase is in equilibrium with bicarbonate, forming a common stock.

The Excel® workbook incorporates a selection feature allowing the user to include or exclude these simplifications and automatically amends the calculations according to the selection. Ignoring CA and assuming a common pool with bicarbonate, the maximum time step scales with the reciprocal of g_S (determining the entrant flow of CO_2) and the model can be used reliably with a 5 ms resolution under a range of conditions.

Future developments

I am currently working on simulating photosynthetic oscillations. This involves adding complexity to the description of CS, new feedback loops, and perhaps allowing multiple timings for signalling functions. Subsequently, I plan to model the triose phosphate utilisation to reproduce the patterns experimentally described by Busch et al. (2017). In the long term, this model will form the core of an emerging C_4 model, encompassing all C_3 features presented here plus a dynamic description of C_4 metabolite diffusion.

In my model, stomatal conductance follows first-order kinetics, but it could be adapted to allow for the sigmoidal kinetics used in other studies (Kirschbaum et al. 1997; Vialet-Chabrand et al. 2013). Another development for the model is the mechanistic implementation of a simplified, dynamic and integrated electron transport chain building on the basis of previous work (Zaks et al. 2012; Laisk and Eichelmann 1989; Zhu et al. 2013; Morales et al. 2018), but including some of the continuous feedbacks present in this model and others (Joliot and Johnson 2011; Roach and Krieger-Liszkay 2014; Foyer et al. 2012).

Shorter processing time could be achieved if all calculations were performed directly using the Excel®-embedded VBA® (Visual Basic for Applications, or another suitable software). This would avoid the need for VBA® and Excel® to interact at every cycle. I choose to keep all the equations in the Excel® workbook to maximise transparency and to allow straightforward model modification and parameterisation without the necessity of modifying the code, which only iterates results. Further gains in processing speed could be achieved by substituting the simple Euler integration, whereby the model is calculated at each time increment, with more sophisticated calculus involving stiff solvers and parallel integration with a range of suitable time steps.

Many of the parameters used to model photosynthesis are temperature dependent. Given the large number of parameters and the difficulty in experimentally resolving the dependency of individual quantities, I opted for not including temperature at this stage, but it should be addressed in the future.

Conclusion

Models are descriptions of natural systems that trade-off comprehensiveness with the simplicity and ease of use. Traditional steady-state models are simple but inherently unsuitable for assessing rapid responses of photosynthesis to environmental drivers. Dynamic models are more complex, but are needed to study rapid responses to environmental perturbation. I derived a dynamic process-based photosynthetic model for C_3 leaves simplifying wherever possible while integrating and expanding the functionalities of recently published dynamic models. In particular, my model combines a hydro-mechanical model of stomatal behaviour with dynamic descriptions of dark and light reactions. The model is presented in a transparent format and can be run as a freely downloadable, stand-alone workbook in Microsoft® Excel®. The model successfully replicated complete gas exchange experiments featuring both short lag times and full photosynthetic acclimation, as well as dynamic transitions

between light, CO_2 and oxygen levels. The model has the potential to supersede steady-state models for detailed or time-dependent ecophysiological studies, and I encourage its use for basic research in photosynthesis. Steady-state models will remain useful for larger scale simulations.

Acknowledgements I am deeply grateful to the Editor of this special issue, Nerea Ubierna Lopez, for editing that improved the clarity and readability, to Joe Quirk for a substantial contribution to writing the first version, I thank Ross Deans (Australian National University, ANU) for unpublished spinach leaf gas exchange data, and Florian Busch (ANU) for help, review, and critical discussion. I am funded through a H2020 Marie Skłodowska-Curie individual fellowship (DILIPHO, ID: 702755).

Compliance with ethical standards

Conflict of interest I have no conflict of interest.

Appendix: model details

Flows

A submodel for light reactions of photosynthetic CO_2 assimilation in C_3 leaves: potential ATP and NADPH production rate

The submodel calculates I_1, I_2, J_1, J_2, J_{ATP} and J_{NADPH} when f_{Cyc}, $f_{Pseudocyc}$, f_Q, f_{NDH}, $Y(II)_{LL}$, s, h, α_V, V_{0V} and θ_V are known. I_1 and I_2 are the light absorbed by PSI and PSII, respectively. J_1 and J_2 are the electron flow though PSI and PSII, respectively. J_{ATP} and J_{NADPH} are the steady-state rates of ATP and NADPH production, respectively. f_{Cyc} is the proportion of electron flow at PSI which follows CEF, $f_{Pseudocyc}$ is the fraction of J_1 used by alternative electron sinks (APX cycle and nitrate reduction), f_Q is the level of Q-cycle engagement, and f_{NDH} is the fraction of f_{Cyc} flowing through NDH. The $Y(II)_{LL}$ is the initial yield of PSII extrapolated under zero PPFD, s is the combined energy partitioning coefficient described in Yin et al. (2009), and h is the number of protons required to synthesise each ATP. α_V, V_{0V} and θ_V, define the slope, the offset and the curvature of the function f'(PPFD), expressing the PPFD dependence of Y(II).

When $f_{Cyc}=0$, I_1, I_2, J_1 and J_2 take the values $I_{1,0}$, $I_{2,0}$, $J_{1,0}$ and $J_{2,0}$, respectively, and $J_{1,0}=J_{2,0}$. Then $I_{2,0}$ and $I_{1,0}$ can be expressed as (Yin et al. 2004, 2009):

$$I_{2,0} = \text{PPFD} \times s, \tag{1}$$

$$I_{1,0} = \frac{I_{2,0}\ Y(\text{II})_{LL}}{Y(\text{I})_{LL}}. \tag{2}$$

The total light absorbed by both PSI and PSII is $I=I_{1,0}+I_{2,0}$ and $I<\text{PPFD}$.

When CEF is engaged, I_1 increases by a quantity χ (Yin et al. 2004):

$$I_1 = (1+\chi)\, I_{1,0}, \tag{3}$$

where χ is calculated as a function of f_{Cyc} as (Yin et al. 2004):

$$\chi = \frac{f_{Cyc}}{1+f_{Cyc}+\ Y(\text{II})_{LL}}. \tag{4a}$$

I simulate the rate of cyclic electron flow through a tentative function as:

$$f_{Cyc} = \max\left(0,\ -1+15^{\ \frac{v\text{ATP}}{J_{ATP}}-\frac{v\text{NADPH}}{J_{NADPH}}}\right). \tag{4b}$$

When the ratio of actual ATP production relative to the potential $\left(\frac{v_{ATP}}{J_{ATP}}\right)$ is greater than the ratio of actual NADPH production relative to the potential $\left(\frac{v_{NADPH}}{J_{NADPH}}\right)$, indicating ATP demand greater than NADPH demand, f_{Cyc} will be greater than zero. Equation 4b yields values very close to zero in C_3 plants, and further testing will be necessary before application with other photosynthetic types.

If I is constant, I_2, J_2 and J_1 are calculated as (Yin et al. 2004):

$$I_2 = \left(\frac{1}{Y(\text{II})_{LL}}-\chi\right) I_{2,0}\ \ Y(\text{II})_{LL}, \tag{5}$$

$$J_2 = I_2\ \ Y(\text{II}), \tag{6}$$

$$J_1 = \frac{J_2}{1-f_{Cyc}}, \tag{7}$$

where Y(II) is the yield of photosystem II, which depends on PPFD and feedbacks from dark reactions through the novel process-based function:

$$Y(\text{II}) = Y(\text{II})_{LL}\ \frac{v\text{ATP}}{J_{ATP}}\ \frac{v\text{NADPH}}{J_{NADPH}}\ \left(1-\max\left[0,\ f'(\text{PPFD})\right]\right). \tag{8}$$

The rationale of Eq. 8 is that Y(II) has a maximum operational value, $Y(II)_{LL}$, and is quenched by three distinct factors (Müller et al. 2001): (1) the slowing down of ATP synthesis caused by limiting availability of phosphate or ADP (described by $\frac{v_{ATP}}{J_{ATP}}$); (2) the reduction of the plastoquinone pool (described by $\frac{v_{NADPH}}{J_{NADPH}}$); (3) reaching the maximum capacity for electron transport (described by f'(PPFD), which responds to PPFD as a non-rectangular hyperbola). f'(PPFD) is calculated with Eq. 20, below, but with different parameterisation, see Table S2. Parameter values were adjusted by fitting modelled assimilation against A/PPFD response curves (Fig. 3, Table S2).

The proton flow to the lumen includes: one proton per electron from water oxidation, one proton from electron flow through the cytochromes (J_{Cyt}), two protons from the electron flow through the Q-cycle (J_Q, Yin et al. 2004) and two protons from the electron flow through NDH ($J_{NDH,}$ Kramer and Evans 2011). The rate of ATP production is:

$$J_{ATP} = \frac{J_2 + J_{Cyt} + 2J_Q + 2J_{NDH}}{h}, \quad (9)$$

where h is the number of protons required to synthesise each ATP molecule, the flow through the Q-cycle is $J_Q = f_Q J_1$; the complement, directly flowing to the b_6f complex, is $J_{Cyt} = (1 - f_Q) J_1$; and the flow through the NDH complex is $J_{NDH} = f_{Cyc} f_{NDH} J_1$.

The total NADPH production can be expressed as (Yin et al. 2004):

$$J_{NADPH} = J_1 \frac{1 - f_{Cyc} - f_{Pseudocyc}}{2}, \quad (10a)$$

The alternative electron sinks include nitrogen metabolism (chiefly reduction) as well as the APX cycle. The APX cycle is known to depend on O_2 concentration and the availability of PSI acceptors (Miyake and Yokota 2000; Schreiber and Neubauer 1990). I describe $f_{Pseudocyc}$ as a linear function of O_2 concentration and $\frac{v_{NADPH}}{J_{NADPH}}$ as:

$$f_{Pseudocyc} = f_{Pseudocyc\ NR} + 4\ [O_2] \left(1 - \frac{v\mathrm{NADPH}}{J_{NADPH}}\right), \quad (10b)$$

where the coefficient 4 was fitted empirically to yield a value of $f_{Pseudocyc} \approx 0.1$ under ordinary ambient conditions, and the fraction of $f_{Pseudocyc}$ partitioned to nitrate reduction ($f_{Pseudocyc\ NR}$) was set at ≈ 0 for simplicity.

The time dependence of J_{ATP} and J_{NADPH} was modelled after Bellasio et al. (2017) as:

$$\begin{cases} J_{ATP\ or\ NADPH\ \ t+dt} = J_{ATP\ or\ NADPH\ t} + \frac{J_{ATP\ or\ NADPH} - J_{ATP\ or\ NADPH\ t}}{K_{J\ ATP\ or\ NADPH}} dt & \text{if } J_{ATP\ or\ NADPH\ t} < J_{ATP\ or\ NADPH} \\ J_{ATP\ or\ NADPH\ t} = J_{ATP\ or\ NADPH} & \text{else} \end{cases}, \quad (11)$$

where $K_{J\ ATP\ or\ NADPH}$ is the time constant for an increase in J_{ATP} or J_{NADPH}, $J_{ATP\ or\ NADPH\ t+dt}$ and $J_{ATP\ or\ NADPH\ t}$ are the values at the time step $t + dt$ or at the previous step t, respectively; $J_{ATP\ or\ NADPH}$ are the steady-state values (Eqs. 9 and 10a).

Actual rates of ATP and NADPH production

The actual rates of ATP (v_{ATP}) and NADPH (v_{NADPH}) production are calculated after Wang et al. (2014b):

$$v_{ATP} = \frac{J_{ATP}\left([ATP][P_i] - \frac{[ADP]}{K_e}\right)}{K_{m\ ADP}K_{m\ P_i}\left(1 + \frac{[ADP]}{K_{m\ ADP}} + \frac{[ATP]}{K_{m\ ATP}} + \frac{[P_i]}{K_{m\ P_i}} + \frac{[ATP][P_i]}{K_{m\ ADP}K_{m\ P_i}}\right)}, \quad (12)$$

$$v_{NADPH} = \frac{J_{NADPH}\left([NADP] - \frac{[NADPH]}{K_e}\right)}{K_{m\ NADP}\left(1 + \frac{[NADP]}{K_{m\ NADP}} + \frac{[NADPH]}{K_{m\ NADPH}}\right)}, \quad (13)$$

where square brackets indicate metabolite concentration, K_m represents the Michaelis–Menten constant for a given metabolite, and K_e is the equilibrium constant of the reaction (Table S1).

CO_2 diffusion, dissolution and hydration

The rate of CO_2 diffusion through the stomata is:

$$CO_2\ \text{stomatal diffusion} = \frac{g_S\left(C_a - C_i\right)}{1000}, \quad (14)$$

where g_S is stomatal conductance to CO_2 (mol m^{-2} s^{-1}); C_a and C_i are the CO_2 concentrations (μmol mol^{-1}) external to the leaf and in the intercellular space, respectively; and the 1000 is used to convert the units from micromoles to mmol m^{-2} s^{-1}.

The rate of CO_2 dissolution in aqueous media within the leaf is:

$$CO_2\ \text{dissolution} = \frac{g_M\left(C_i - [CO_2]K_{hCO_2}\right)}{1000}, \quad (15)$$

where g_M is mesophyll conductance to CO_2 diffusion (mol m^{-2} s^{-1}), $[CO_2]$ is the CO_2 concentration in mesophyll cells (mM), which is assumed to be spatially uniform, K_{hCO_2} is CO_2 volatility (the reciprocal of solubility) (μbar mM^{-1}) and 1000 is used to convert the units into mmol m^{-2} s^{-1}, the unit of all subsequent rates.

The rate of CO_2 hydration to bicarbonate is (Wang et al. 2014b):

$$CA = \frac{V_{MAX\ CA}\left([CO_2] - \frac{[HCO_3^-][H^+]}{K_e}\right)}{K_{m\ CO_2}\left(1 + \frac{[CO_2]}{K_{m\ CO_2}} + \frac{[HCO_3^-]}{K_{m\ HCO_3}}\right)}, \quad (16)$$

where $V_{MAX\ CA}$ is the maximum hydration rate.

Reaction rates

The rate of Rubisco carboxylation (V_C) was modified from Wang et al. (2014b) as:

$$V_C = \frac{V_{C\,MAX}\ R_{act}\ f(\text{RuBP})\ [\text{RuBP}]\left[CO_2\right]}{\left(K'_{m\,CO_2} + \left[CO_2\right]\right)\left(K'_{m\,RuBP} + [\text{RuBP}]\right)}, \tag{17}$$

where $V_{C\,MAX}$ is the maximum carboxylation rate. In the $V_{C\,MAX}$ used in Farquhar et al. (1980), Rubisco is assumed fully activated and also fully RuBP saturated in the 'enzyme-limited' case. Here, $V_{C\,MAX}$ is more closely comparable to the in vitro rate. R_{act} is the Rubisco activation state, a time-dependent variable calculated as:

$$R_{act\ t+dt} = R_{act\ t} + \begin{cases} \frac{R_{act\ eq} - R_{act\ t}}{\tau_i}\ dt & \text{if } R_{act\ t} < R_{act\ eq} \\ \frac{R_{act\ eq} - R_{act\ t}}{\tau_d}\ dt & \text{else} \end{cases}, \tag{18}$$

where τ_i and τ_d are the time constants for Rubisco induction and deactivation, respectively (Seemann et al. 1988), and the steady state R_{act} value is:

$$R_{act} = f(\text{PPFD})\ \ f\left(\left[CO_2\right]\right), \tag{19}$$

where f(PPFD) simulates activation state of Rubisco independently of CO_2 concentration, and I included $f([CO_2])$ to capture the inactivation of Rubisco observed in vivo at low CO_2. The f(PPFD) and $f([CO_2])$ were modelled with non-rectangular hyperbolas (Gross et al. 1991):

$$f(\text{PPFD}) = V_0 + \frac{\alpha_V\ \text{PPFD} + 1 - V_0 - \sqrt{\left(\alpha_V\ \text{PPFD} + 1 - V_0\right)^2 - 4\alpha_V\ \text{PPFD}\ \theta_V}}{2\ \theta_V}, \tag{20}$$

$$f\left(\left[CO_2\right]\right) = V_{0C} + \frac{\alpha_C\ \left[CO_2\right] + 1 - V_{0C} - \sqrt{\left(\alpha_V\ \left[CO_2\right] + 1 - V_{0C}\right)^2 - 4\alpha_C\ \left[CO_2\right]\ \theta_C}}{2\ \theta_C}, \tag{21}$$

where V_0, α_V, and θ_V are empirical parameters of the hyperbola for f(PPFD) defining the initial activity in the dark, the slope of the dependency and the curvature, respectively; V_{0C}, α_C, and θ_C are the equivalent parameters for $f([CO_2])$.

The f(RuBP) is a function of RuBP concentration, relative to the concentration of Rubisco active sites, which was modelled using a non-rectangular hyperbola after Farquhar et al. (1980):

$$f(\text{RuBP}) = \frac{E_T + K'_{m\,RuBP} + [\text{RuBP}] - \sqrt{\left(E_T + K'_{m\,RuBP} + [\text{RuBP}]\right)^2 - 4[\text{RuBP}]E_T}}{2E_T}, \tag{22}$$

where E_T is the total concentration of Rubisco catalytic sites, calculated from $V_{C\,MAX}$ and turnover rate after Wang et al. (2014b). The Michaelis–Menten constant for RuBP and CO_2 are:

$$K'_{m\,RuBP} = K_{m\,RuBP}\left(1 + \frac{[\text{PGA}]}{K_{m\,PGA}} + \frac{[\text{NADP}]}{K_{i\,NADP}} + \frac{[\text{ADP}]}{K_{i\,ADP}} + \frac{[P_i]}{K_{i\,P_i}}\right), \tag{23}$$

$$K'_{m\,CO_2} = K_{m\,CO_2}\left(1 + \frac{[O_2]}{K_{m\,O_2}}\right), \tag{24}$$

where K_i are the constants for the competitive inhibition.

The rate of Rubisco oxygenation (V_O) was calculated after Farquhar et al. (1980) as:

$$V_O = V_C\ 2\gamma^*\ \frac{[O_2]}{[CO_2]}, \tag{25}$$

where γ^* is half the reciprocal Rubisco specificity, calculated in the liquid phase (von Caemmerer 2000) using constants from Sander (2015) and Warneck and Williams (2012). In this model, the glycine decarboxylase (GDC) decarboxylation rate equals V_O; for a justification and possible stoichiometric variants, see Bellasio (2017).

The rate of RuP phosphorylation was modified from Wang et al. (2014b) as:

$$\mathrm{RuP_{Phosp}} = \frac{V_{\mathrm{MAX}}\ [\mathrm{ATP}][\mathrm{RuP}]\ -\frac{[\mathrm{ATP}][\mathrm{RuBP}]}{K_{\mathrm{e}}}}{\left([\mathrm{ATP}]\ +\ K_{\mathrm{m\ ATP}}\left(1+\ \frac{[\mathrm{ADP}]}{K_{\mathrm{i\ ADP}}}\right)\right)\left([\mathrm{RuP}]+K_{\mathrm{m\ RuP}}\left(1+\ \frac{[\mathrm{PGA}]}{K_{\mathrm{i\ PGA}}}\ +\ \frac{[\mathrm{RuBP}]}{K_{\mathrm{i\ RuBP}}}\ +\ \frac{[P_{\mathrm{i}}]}{K_{\mathrm{i}\ P_{\mathrm{i}}}}\right)\right)}. \tag{26}$$

The reducing phase of the reductive pentose phosphate pathway was modelled as a single-step pseudoreaction. The rate of PGA reduction (PR) was calculated by fusing the rates of PGA phosphorylation and DPGA reduction from Wang et al. (2014b) as:

$$\mathrm{PR} = \frac{V_{\mathrm{MAX}}\ [\mathrm{ATP}][\mathrm{PGA}][\mathrm{NADPH}]}{\left([\mathrm{PGA}]\ +\ K_{\mathrm{m\ PGA}}\left(1+\ \frac{[\mathrm{ADP}]}{K_{\mathrm{i\ ADP}}}\right)\right)\left([\mathrm{ATP}]\ +\ K_{\mathrm{m\ ATP}}\left(1+\ \frac{[\mathrm{ADP}]}{K_{\mathrm{i\ ADP}}}\right)\right)\left([\mathrm{NADPH}]\ +\ K_{\mathrm{m\ NADPH}}\left(1+\ \frac{[\mathrm{ADP}]}{K_{\mathrm{i\ ADP}}}\right)\right)}. \tag{27}$$

The constants in Eq. 27 were adapted from the original separate reactions in Wang et al. (2014b) to maintain physiologically realistic concentrations of product and substrates. This was necessary to account for neglecting phosphorylated intermediates of the RPP.

Carbohydrate synthesis was assumed to be a single-step reaction, and the rate was calculated by simplifying the combined processes of starch and sucrose synthesis from Wang et al. (2014b) as:

$$\mathrm{CS} = \frac{V_{\mathrm{MAX}}\ ([\mathrm{DHAP}]-0.4)\left(1-\frac{|\mathrm{PR}|\ [P_{\mathrm{i}}]}{K_{\mathrm{e}}}\right)}{\left([\mathrm{DHAP}]\ +\ K_{\mathrm{m\ DHAP}}\left(1+\ \frac{[\mathrm{ADP}]}{K_{\mathrm{i\ ADP}}}\right)\right)}. \tag{28a}$$

With Eq. 28a carbohydrates are synthesised when [DHAP] > 0.4 mM following a saturating Michaelis–Menten kinetics, inhibited by ADP. Concentration of sucrose, starch and their precursor are not calculated. To capture the reversible nature of the original Wang et al. (2014b) formulation, I use the quantity $\frac{|\mathrm{PR}|\ [P_{\mathrm{i}}]}{K_{\mathrm{e}}}$, where |PR| 'senses' the concentration of sucrose and starch, hypothesised to be proportional to the rate of DHAP synthesis.

The interconversion phase of the RPP was modelled as a single-step pseudoreaction through a generic Michaelis Menten equation for equilibrium reaction (Zhu et al. 2007) as:

$$\mathrm{RPP}=\frac{V_{\mathrm{MAX}}\ [\mathrm{DHAP}]\ \left(1-\frac{|\mathrm{RuP}|}{K_{\mathrm{e}}}\right)}{\left([\mathrm{DHAP}]+K_{\mathrm{m\ DHAP}}\right)}. \tag{28b}$$

The constants in Eq. 28b were adapted from the original separate reactions in Wang et al. (2014b) to operate and maintain physiologically realistic concentrations of substrates.

Stocks

Change in metabolite concentrations

The change in metabolite concentrations in time $\frac{\mathrm{d}[]}{\mathrm{d}t}$ was described by a set of ordinary differential equations based on the stoichiometry of Bellasio (2017) informed with the reaction rates described above and converted from variation in leaf-level pool to variation in concentration using the mesophyll volume as described in Wang et al. (2014b).

The rates of change in concentrations of CO_2, bicarbonate (HCO_3^-), RuBP, PGA, DHAP, ATP and NADPH were calculated as:

$$\frac{\mathrm{d}[\mathrm{CO_2}]}{\mathrm{d}t}V_{\mathrm{M}} = \mathrm{CO_2\ Dissolution} + R_{\mathrm{LIGHT}} - V_{\mathrm{C}} + 0.5\ \mathrm{GDC} - \mathrm{CA}, \tag{29}$$

$$\frac{\mathrm{d}[\mathrm{HCO_3^-}]}{\mathrm{d}t}V_{\mathrm{M}} = \mathrm{CA}, \tag{30}$$

$$\frac{\mathrm{d}[\mathrm{RuBP}]}{\mathrm{d}t}V_{\mathrm{M}} = \mathrm{RuP_{Phosp}} - V_{\mathrm{C}} - V_{\mathrm{O}}, \tag{31}$$

$$\frac{\mathrm{d}[\mathrm{PGA}]}{\mathrm{d}t}V_{\mathrm{M}} = 2\ V_{\mathrm{C}} + V_{\mathrm{O}} + 0.5\ \mathrm{GDC} - \mathrm{PR} - \frac{1}{3}R_{\mathrm{LIGHT}}, \tag{32}$$

$$\frac{\mathrm{d}[\mathrm{DHAP}]}{\mathrm{d}t}V_{\mathrm{M}} = \mathrm{PR} - \mathrm{CS} - \frac{5}{3}\mathrm{RuP_{Phosp}}, \tag{33}$$

$$\frac{\mathrm{d}[\mathrm{ATP}]}{\mathrm{d}t}V_{\mathrm{M}} = v_{\mathrm{ATP}} - \mathrm{RuP_{Phosp}} - V_{\mathrm{O}} - \mathrm{PR} - 0.5\ \mathrm{CS}, \tag{34}$$

$$\frac{\mathrm{d}[\mathrm{NADPH}]}{\mathrm{d}t}V_{\mathrm{M}} = v_{\mathrm{NADPH}} - \mathrm{PR} - 0.5\ V_{\mathrm{O}}, \tag{35}$$

$$\frac{\mathrm{d}[\mathrm{RuP}]}{\mathrm{d}t}V_{\mathrm{M}} = \mathrm{RPP} - \mathrm{RuP_{Phosp}}, \tag{36}$$

where V_{M} is mesophyll volume per meter square of leaf (L m^{-2}) calculated after considering the leaf half-full of mesophyll (Lawlor 1993), R_{LIGHT} is light respiration and is

input to the model as described in Bellasio (2017), and all the other flux rates have been previously described: CO_2 dissolution (Eq. 15), CA (Eq. 16), RuP_{Phosph} (Eq. 26), V_C (Eq. 17), V_O (=GDC, Eq. 25), PR (Eq. 27), CS (Eq. 28a), v_{ATP} (Eq. 12), v_{NADPH} (Eq. 13) and RPP (Eq. 28b). Equations 29–30 were derived in this study and Eqs. 31–36 are modified from (Bellasio 2017).

Concentrations determined from total metabolite pools

The concentrations of ADP, $NADP^+$ and phosphate ($[P_i]$) are calculated simply by subtraction from a total pool:

$$[\mathrm{ADP}] = A_{\mathrm{Tot}} - [\mathrm{ATP}], \tag{37}$$

$$\left[\mathrm{NADP}^+\right] = N_{\mathrm{Tot}} - [\mathrm{NADPH}], \tag{38}$$

$$[P_i] = P_{i\mathrm{Tot}} - [\mathrm{PGA}] - [\mathrm{DHAP}] - [\mathrm{RuP}] - 2[\mathrm{RuBP}] - [\mathrm{ATP}], \tag{39}$$

where A_{Tot}, N_{Tot}, and P_{iTot} are the total pools of adenylates, nicotinamides and phosphate, respectively.

The hydro-mechanical model of stomatal behaviour

The model calculates g_S after Bellasio et al. (2017) as:

$$g_S = \max\left(g_{S\,0},\ \frac{\chi\ \beta\ \tau\ \left(\Psi_{\mathrm{Soil}} + \pi_e\right)}{1 + \chi\ \beta\ \tau\ R_h\ D_S}\right), \tag{40}$$

where $\chi\beta$ is a combined parameter scaling turgor-to-conductance and the hydro-mechanical-to-biochemical response; τ is the sensor of biochemical forcing; Ψ_{Soil} is soil water potential; π_e is epidermal osmotic pressure; R_h is the effective hydraulic resistance to the epidermis, calculated as $1/K_h$, the corresponding hydraulic conductance; and D_S is the leaf-to-boundary layer H_2O mole fraction gradient, a measure of vapour pressure deficit, VPD. The parameter τ encompasses the biochemical components of the model and is calculated from f(RuBP) as:

$$\tau = \tau_0 + f(\mathrm{RuBP}), \tag{41}$$

where τ_0, the basal level of τ, was manually assigned. Stomatal dynamics were accounted for by describing the time dependence of g_S with a set of recursive equations (Bellasio et al. 2017):

$$g_{S\,t+\mathrm{d}t} = g_{S\,t} + \begin{cases} \frac{g_S - g_{S\,t}}{K_i}\,\mathrm{d}t & \text{if } g_{S\,t} < g_S \\ \frac{g_S - g_{S\,t}}{K_d}\,\mathrm{d}t & \text{else} \end{cases}, \tag{42}$$

where g_{St+dt} and g_{St} are the g_S values at the time step $t+dt$ or at the previous step t, respectively; g_S is the steady-state value (Eq. 40), K_i and K_d are the time constants for an increase and decrease in g_S, respectively.

References

Allen WA, Richardson AJ (1968) Interaction of light with a plant canopy. J Opt Soc Am 58(8):1023–1028. https://doi.org/10.1364/Josa.58.001023

Beerling DJ (2015) Gas valves, forests and global change: a commentary on Jarvis (1976) 'The interpretation of the variations in leaf water potential and stomatal conductance found in canopies in the field'. Philos Trans R Soc B. https://doi.org/10.1098/rstb.2014.0311

Bellasio C (2017) A generalised stoichiometric model of C3, C2, C2 + C4, and C4 photosynthetic metabolism. J Exp Bot 68(2):269–282. https://doi.org/10.1093/jxb/erw303

Bellasio C, Griffiths H (2014) The operation of two decarboxylases (NADPME and PEPCK), transamination and partitioning of C4 metabolic processes between mesophyll and bundle sheath cells allows light capture to be balanced for the maize C4 pathway. Plant Physiol 164:466–480. https://doi.org/10.1111/pce.12194

Bellasio C, Burgess SJ, Griffiths H, Hibberd JM (2014) A high throughput gas exchange screen for determining rates of photorespiration or regulation of C4 activity. J Exp Bot 65(13):3769–3779. https://doi.org/10.1093/jxb/eru238

Bellasio C, Beerling DJ, Griffiths H (2016a) Deriving C_4 photosynthetic parameters from combined gas exchange and chlorophyll fluorescence using an Excel tool: theory and practice. Plant Cell Environment 39(6):1164–1179. https://doi.org/10.1111/pce.12626

Bellasio C, Beerling DJ, Griffiths H (2016b) An Excel tool for deriving key photosynthetic parameters from combined gas exchange and chlorophyll fluorescence: theory and practice. Plant Cell Environ 39(6):1180–1197. https://doi.org/10.1111/pce.12560

Bellasio C, Quirk J, Buckley TN, Beerling D (2017) A dynamic hydromechanical and biochemical model of stomatal conductance for C4 photosynthesis. Plant Physiol. https://doi.org/10.1104/pp.17.00666

Berry JA, Beerling DJ, Franks PJ (2010) Stomata: key players in the earth system, past and present. Curr Opin Plant Biol 13(3):232–239. https://doi.org/10.1016/j.pbi.2010.04.013

Bonan GB, Williams M, Fisher RA, Oleson KW (2014) Modeling stomatal conductance in the earth system: linking leaf water-use efficiency and water transport along the soil–plant–atmosphere continuum. Geosci Model Dev 7(5):2193–2222. https://doi.org/10.5194/gmd-7-2193-2014

Buckley TN (2017) Modeling stomatal conductance. Plant Physiol. https://doi.org/10.1104/pp.16.01772

Buckley TN, Mott KA, Farquhar GD (2003) A hydromechanical and biochemical model of stomatal conductance. Plant Cell Environ 26(10):1767–1785. https://doi.org/10.1046/j.1365-3040.2003.01094.x

Busch FA (2014) Opinion: the red-light response of stomatal movement is sensed by the redox state of the photosynthetic electron transport chain. Photosynth Res 119(1–2):131–140. https://doi.org/10.1007/s11120-013-9805-6

Busch FA, Sage RF (2017) The sensitivity of photosynthesis to O_2 and CO_2 concentration identifies strong Rubisco control above the thermal optimum. New Phytol 213(3):1036–1051. https://doi.org/10.1111/nph.14258

Busch FA, Sage RF, Farquhar GD (2017) Plants increase CO_2 uptake by assimilating nitrogen via the photorespiratory pathway. Nat Plants. https://doi.org/10.1038/s41477-017-0065-x

Damour G, Simonneau T, Cochard H, Urban L (2010) An overview of models of stomatal conductance at the leaf level. Plant Cell Environ 33(9):1419–1438. https://doi.org/10.1111/j.1365-3040.2010.02181.x

Davis PA, Caylor S, Whippo CW, Hangarter RP (2011) Changes in leaf optical properties associated with light-dependent chloroplast movements. Plant Cell Environ 34(12):2047–2059

Driever SM, Simkin AJ, Alotaibi S, Fisk SJ, Madgwick PJ, Sparks CA, Jones HD, Lawson T, Parry MAJ, Raines CA (2017) Increased SBPase activity improves photosynthesis and grain yield in wheat grown in greenhouse conditions. Philos Trans R Soc B. https://doi.org/10.1098/rstb.2016.0384

Farquhar G, Wong S (1984) An empirical model of stomatal conductance. Funct Plant Biol 11(3):191–210. https://doi.org/10.1071/PP9840191

Farquhar GD, von Caemmerer S, Berry JA (1980) A biochemical-model of photosynthetic CO_2 assimilation in leaves of C3 species. Planta 149(1):78–90. https://doi.org/10.1007/bf00386231

Foyer CH, Lelandais M, Harbinson J (1992) Control of the quantum efficiencies of photosystems I and II, electron flow, and enzyme activation following dark-to-light transitions in pea leaves: relationship between NADP/NADPH ratios and NADP-malate dehydrogenase activation state. Plant Physiol 99(3):979–986

Foyer CH, Neukermans J, Queval G, Noctor G, Harbinson J (2012) Photosynthetic control of electron transport and the regulation of gene expression. J Exp Bot 63(4):1637–1661. https://doi.org/10.1093/jxb/ers013

Gross LJ (1982) Photosynthetic dynamics in varying light environments: a model and its application to whole leaf carbon gain. Ecology 63(1):84–93

Gross LJ, Kirschbaum MUF, Pearcy RW (1991) A dynamic-model of photosynthesis in varying light taking account of stomatal conductance, C3-cycle intermediates, photorespiration and rubisco activation. Plant Cell Environ 14(9):881–893. https://doi.org/10.1111/j.1365-3040.1991.tb00957.x

Heineke D, Riens B, Grosse H, Hoferichter P, Peter U, Flügge U-I, Heldt HW (1991) Redox transfer across the inner chloroplast envelope membrane. Plant Physiol 95(4):1131–1137

Hendrey G, Long S, McKee I, Baker N (1997) Can photosynthesis respond to short-term fluctuations in atmospheric carbon dioxide? Photosynth Res 51(3):179–184

Ho QT, Berghuijs HNC, WattÉ R, Verboven P, Herremans ELS, Yin X, Retta MA, Aernouts BEN, Saeys W, Helfen L, Farquhar GD, Struik PC, NicolaÏ BM (2015) Three-dimensional microscale modelling of CO_2 transport and light propagation in tomato leaves enlightens photosynthesis. Plant Cell Environ. https://doi.org/10.1111/pce.12590

Ishikawa N, Takabayashi A, Sato F, Endo T (2016) Accumulation of the components of cyclic electron flow around photosystem I in C4 plants, with respect to the requirements for ATP. Photosynth Res. https://doi.org/10.1007/s11120-016-0251-0

Joliot P, Johnson GN (2011) Regulation of cyclic and linear electron flow in higher plants. Proc Natl Acad Sci 108(32):13317–13322. https://doi.org/10.1073/pnas.1110189108

Kaiser E, Morales A, Harbinson J, Kromdijk J, Heuvelink E, Marcelis LFM (2014) Dynamic photosynthesis in different environmental conditions. J Exp Bot. https://doi.org/10.1093/jxb/eru406

Kirschbaum M, Küppers M, Schneider H, Giersch C, Noe S (1997) Modelling photosynthesis in fluctuating light with inclusion of stomatal conductance, biochemical activation and pools of key photosynthetic intermediates. Planta 204(1):16–26

Kramer DM, Evans JR (2011) The importance of energy balance in improving photosynthetic productivity. Plant Physiol 155(1):70–78. https://doi.org/10.1104/pp.110.166652

Kromdijk J, Głowacka K, Leonelli L, Gabilly ST, Iwai M, Niyogi KK, Long SP (2016) Improving photosynthesis and crop productivity by accelerating recovery from photoprotection. Science 354(6314):857–861. https://doi.org/10.1126/science.aai8878

Laisk A, Edwards GE (2000) A mathematical model of C4 photosynthesis: the mechanism of concentrating CO_2 in NADP-malic enzyme type species. Photosynth Res 66(3):199–224. https://doi.org/10.1023/a:1010695402963

Laisk A, Edwards G (2009) Leaf C4 photosynthesis in silico: the CO_2 concentrating mechanism. In: Laisk A, Nedbal L, Govindjee (eds) Photosynthesis in silico, vol 29. Advances in photosynthesis and respiration. Springer, Amsterdam, pp 323–348. https://doi.org/10.1007/978-1-4020-9237-4_14

Laisk A, Eichelmann H (1989) Towards understanding oscillations: a mathematical model of the biochemistry of photosynthesis. Phil Trans R Soc Lond B 323(1216):369–384

Laisk A, Eichelmann H, Oja V, Eatherall A, Walker DA (1989) A mathematical model of the carbon metabolism in photosynthesis. Difficulties in explaining oscillations by fructose 2, 6-bisphosphate regulation. Proc R Soc Lond B 237(1289):389–415

Laisk A, Siebke K, Gerst U, Eichelmann H, Oja V, Heber U (1991) Oscillations in photosynthesis are initiated and supported by imbalances in the supply of ATP and NADPH to the Calvin cycle. Planta 185(4):554–562. https://doi.org/10.1007/bf00202966

Laisk A, Eichelmann H, Oja V (2009) Leaf C3 photosynthesis in silico: integrated carbon/nitrogen metabolism. In: Laisk A, Nedbal L, Govindjee (eds) Photosynthesis in silico, vol 29. Advances in photosynthesis and respiration. Springer, Amsterdam, pp 295–322. https://doi.org/10.1007/978-1-4020-9237-4_13

Lawlor DW (1993) Photosynthesis: molecular, physiological and environmental processes, 2nd edn. Longman Scientific & Technical, Harlow

Lawson T, Blatt MR (2014) Stomatal size, speed, and responsiveness impact on photosynthesis and water use efficiency. Plant Physiol 164(4):1556–1570. https://doi.org/10.1104/pp.114.237107

Lehmeier C, Pajor R, Lundgren MR, Mathers A, Sloan J, Bauch M, Mitchell A, Bellasio C, Green A, Bouyer D, Schnittger A, Sturrock C, Osborne CP, Rolfe S, Mooney S, Fleming AJ (2017) Cell density and airspace patterning in the leaf can be manipulated to increase leaf photosynthetic capacity. Plant J 92(6):981–994. https://doi.org/10.1111/tpj.13727

Long SP (1993) The significance of light-limited photosynthesis to crop canopy carbon gain and productivity—a theoretical analysis. In: Abrol YP, Mohanty P, Govindjee (eds) Photosynthesis: photoreactions to plant productivity. Oxford & IBH Publishing, New Delhi, pp 547–560

Long SP, Farage PK, Garcia RL (1996) Measurement of leaf and canopy photosynthetic CO_2 exchange in the field. J Exp Bot 47(304):1629–1642. https://doi.org/10.1093/jxb/47.11.1629

Long SP, Ainsworth EA, Leakey ADB, Nösberger J, Ort DR (2006) Food for thought: Lower-than-expected crop yield stimulation with rising CO_2 concentrations. Science 312(5782):1918–1921. https://doi.org/10.1126/science.1114722

Long SP, Marshall-Colon A, Zhu X-G (2015) Meeting the global food demand of the future by engineering crop photosynthesis and yield potential. Cell 161(1):56–66. https://doi.org/10.1016/j.cell.2015.03.019

McAusland L, Vialet-Chabrand S, Davey P, Baker NR, Brendel O, Lawson T (2016) Effects of kinetics of light-induced stomatal responses on photosynthesis and water-use efficiency. New Phytol 211(4):1209–1220. https://doi.org/10.1111/nph.14000

McQualter RB, Bellasio C, Gebbie L, Petrasovits LA, Palfreyman R, Hodson M, Plan M, Blackman D, Brumbley S, Nielsen L (2016) Systems biology and metabolic modelling unveils limitations to polyhydroxybutyrate accumulation in sugarcane leaves; lessons for C4 engineering. Plant Biotechnol J 14(2):567–580. https://doi.org/10.1111/pbi.12399

Messinger SM, Buckley TN, Mott KA (2006) Evidence for involvement of photosynthetic processes in the stomatal response to CO_2. Plant Physiol 140(2):771–778. https://doi.org/10.1104/pp.105.073676

Miyake C, Yokota A (2000) Determination of the rate of photoreduction of O_2 in the water-water cycle in watermelon leaves and enhancement of the rate by limitation of photosynthesis. Plant Cell Physiol 41(3):335–343

Morales A, Kaiser E, Yin X, Harbinson J, Molenaar J, Driever SM, Struik PC (2018) Dynamic modelling of limitations on improving leaf CO_2 assimilation under fluctuating irradiance. Plant Cell Environ 41(3):589–604. https://doi.org/10.1111/pce.13119

Mott KA, Berg DG, Hunt SM, Peak D (2014) Is the signal from the mesophyll to the guard cells a vapour-phase ion? Plant Cell Environ 37(5):1184–1191. https://doi.org/10.1111/pce.12226

Müller P, Li X-P, Niyogi KK (2001) Non-photochemical quenching. A response to excess light energy. Plant Physiol 125(4):1558–1566

Naumburg E, Ellsworth DS (2002) Short-term light and leaf photosynthetic dynamics affect estimates of daily understory photosynthesis in four tree species. Tree Physiol 22(6):393–401. https://doi.org/10.1093/treephys/22.6.393

Ostle NJ, Smith P, Fisher R, Ian Woodward F, Fisher JB, Smith JU, Galbraith D, Levy P, Meir P, McNamara NP, Bardgett RD (2009) Integrating plant–soil interactions into global carbon cycle models. J Ecol 97(5):851–863. https://doi.org/10.1111/j.1365-2745.2009.01547.x

Pearcy RW (1990) Sunflecks and photosynthesis in plant canopies. Annu Rev Plant Physiol Plant Mol Biol 41(1):421–453. https://doi.org/10.1146/annurev.pp.41.060190.002225

Pearcy RW, Osteryoung K, Calkin HW (1985) Photosynthetic responses to dynamic light environments by Hawaiian trees: time course of CO_2 uptake and carbon gain during sunflecks. Plant Physiol 79(3):896–902. https://doi.org/10.1104/pp.79.3.896

Pearcy RW, Gross LJ, He D (1997) An improved dynamic model of photosynthesis for estimation of carbon gain in sunfleck light regimes. Plant Cell Environ 20(4):411–424. https://doi.org/10.1046/j.1365-3040.1997.d01-88.x

Portis AR, Salvucci ME, Ogren WL (1986) Activation of ribulosebisphosphate carboxylase/oxygenase at physiological CO_2 and ribulosebisphosphate concentrations by Rubisco activase. Plant Physiol 82(4):967–971

Ray DK, Ramankutty N, Mueller ND, West PC, Foley JA (2012) Recent patterns of crop yield growth and stagnation. Nat Commun 3:1293. https://doi.org/10.1038/ncomms2296

Ray DK, Mueller ND, West PC, Foley JA (2013) Yield trends are insufficient to double global crop production by 2050. PLoS ONE 8(6):e66428. https://doi.org/10.1371/journal.pone.0066428

Retta M, Ho QT, Yin X, Verboven P, Berghuijs HNC, Struik PC, Nicolaï BM (2016) A two-dimensional microscale model of gas exchange during photosynthesis in maize (*Zea mays* L.) leaves. Plant Sci 246(Supplement C):37–51. https://doi.org/10.1016/j.plantsci.2016.02.003

Roach T, Krieger-Liszkay A (2014) Regulation of photosynthetic electron transport and photoinhibition. Curr Protein Pept Sci 15(4):351–362

Rodriguez-Dominguez CM, Buckley TN, Egea G, de Cires A, Hernandez-Santana V, Martorell S, Diaz-Espejo A (2016) Most stomatal closure in woody species under moderate drought can be explained by stomatal responses to leaf turgor. Plant Cell Environ 39(9):2014–2026. https://doi.org/10.1111/pce.12774

Sage RF, Cen Y-P, Li M (2002) The activation state of Rubisco directly limits photosynthesis at low CO_2 and low O_2 partial pressures. Photosynth Res 71(3):241. https://doi.org/10.1023/a:1015510005536

Sander R (2015) Compilation of Henry's law constants (version 4.0) for water as solvent. Atmos Chem Phys 15(8):4399–4981. https://doi.org/10.5194/acp-15-4399-2015

Santarius KA, Heber U (1965) Changes in the intracellular levels of ATP, ADP, AMP and Pi and regulatory function of the adenylate system in leaf cells during photosynthesis. Biochim Biophys Acta (BBA): Biophys Incl Photosyn 102 (1):39–54. https://doi.org/10.1016/0926-6585(65)90201-3

Sato H, Kumagai TO, Takahashi A, Katul GG (2015) Effects of different representations of stomatal conductance response to humidity across the African continent under warmer CO_2-enriched climate conditions. J Geophys Res: Biogeosci 120(5):979–988. https://doi.org/10.1002/2014JG002838

Schreiber U, Neubauer C (1990) O_2-dependent electron flow, membrane energization and the mechanism of non-photochemical quenching of chlorophyll fluorescence. Photosynth Res 25(3):279–293

Seemann JR, Kirschbaum MU, Sharkey TD, Pearcy RW (1988) Regulation of ribulose-1, 5-bisphosphate carboxylase activity in *Alocasia macrorrhiza* in response to step changes in irradiance. Plant Physiol 88(1):148–152

Song Q, Zhang G, Zhu X-G (2013) Optimal crop canopy architecture to maximise canopy photosynthetic CO_2 uptake under elevated CO_2-a theoretical study using a mechanistic model of canopy photosynthesis. Funct Plant Biol 40(2):108–124. https://doi.org/10.1071/FP12056

Taylor SH, Long SP (2017) Slow induction of photosynthesis on shade to sun transitions in wheat may cost at least 21% of productivity. Philos Trans R Soc B. https://doi.org/10.1098/rstb.2016.0543

Tholen D, Ethier G, Genty B, Pepin S, Zhu XG (2012) Variable mesophyll conductance revisited: theoretical background and experimental implications. Plant Cell Environ 35(12):2087–2103

Trinkunas G, Connelly JP, Müller MG, Valkunas L, Holzwarth AR (1997) Model for the excitation dynamics in the light-harvesting complex II from higher plants. J Phys Chem B 101(37):7313–7320. https://doi.org/10.1021/jp963968j

Valladares F, Allen MT, Pearcy RW (1997) Photosynthetic responses to dynamic light under field conditions in six tropical rainforest shrubs occurring along a light gradient. Oecologia 111(4):505–514. https://doi.org/10.1007/s004420050264

Vialet-Chabrand S, Dreyer E, Brendel O (2013) Performance of a new dynamic model for predicting diurnal time courses of stomatal conductance at the leaf level. Plant Cell Environ 36(8):1529–1546

Vialet-Chabrand S, Matthews JSA, Brendel O, Blatt MR, Wang Y, Hills A, Griffiths H, Rogers S, Lawson T (2016) Modelling water use efficiency in a dynamic environment: an example using *Arabidopsis thaliana*. Plant Sci 251:65–74. https://doi.org/10.1016/j.plantsci.2016.06.016

von Caemmerer S (2000) Biochemical models of leaf photosynthesis. Techniques in plant science. CSIRO Publishing, Collingwood

von Caemmerer S, Edmondson DL (1986) Relationship between steady-state gas-exchange, invivo ribulose bisphosphate carboxylase activity and some carbon-reduction cycle intermediates in *Raphanus-sativus*. Aust J Plant Physiol 13(5):669–688

Walker D (1992) Concerning oscillations. Photosynth Res 34(3):387–395

Wang Y, Bräutigam A, Weber APM, Zhu X-G (2014a) Three distinct biochemical subtypes of C4 photosynthesis? A modelling analysis. J Exp Bot. https://doi.org/10.1093/jxb/eru058

Wang Y, Long SP, Zhu X-G (2014b) Elements required for an efficient NADP-malic enzyme type C4 photosynthesis. Plant Physiol 164(4):2231–2246. https://doi.org/10.1104/pp.113.230284

Wang S, Tholen D, Zhu X-G (2017) C4 photosynthesis in C3 rice: a theoretical analysis of biochemical and anatomical factors. Plant Cell Environ 40(1):80–94. https://doi.org/10.1111/pce.12834

Warneck P, Williams J (2012) Rate coefficients for gas-phase reactions. In: the atmospheric chemist's companion. Springer, Amsterdam, pp 227–269

Way DA, Pearcy RW (2012) Sunflecks in trees and forests: from photosynthetic physiology to global change biology. Tree Physiol 32(9):1066–1081. https://doi.org/10.1093/treephys/tps064

Way DA, Oren R, Kim HS, Katul GG (2011) How well do stomatal conductance models perform on closing plant carbon budgets? A test using seedlings grown under current and elevated air temperatures. J Geophys Res: Biogeosci (2005–2012). https://doi.org/10.1029/2011JG001808

Wong SC (1979) Elevated atmospheric partial-pressure of CO_2 and plant-growth.1. Interactions of nitrogen nutrition and photosynthetic capacity in C_3 and C_4 plants. Oecologia 44(1):68–74. https://doi.org/10.1007/Bf00346400

Yamori W, Shikanai T (2016) Physiological functions of cyclic electron transport around photosystem I in sustaining photosynthesis and plant growth. Annu Rev Plant Biol 67(1):81–106. https://doi.org/10.1146/annurev-arplant-043015-112002

Yin XY, Struik PC (2012) Mathematical review of the energy transduction stoichiometries of C4 leaf photosynthesis under limiting light. Plant Cell Environ 35(7):1299–1312. https://doi.org/10.1111/j.1365-3040.2012.02490.x

Yin X, Van Oijen M, Schapendonk A (2004) Extension of a biochemical model for the generalized stoichiometry of electron transport limited C3 photosynthesis. Plant Cell Environ 27(10):1211–1222

Yin X, Struik PC, Romero P, Harbinson J, Evers JB, Van Der Putten PEL, Vos JAN (2009) Using combined measurements of gas exchange and chlorophyll fluorescence to estimate parameters of a biochemical C_3 photosynthesis model: a critical appraisal and a new integrated approach applied to leaves in a wheat (Triticum aestivum) canopy. Plant Cell Environ 32(5):448–464. https://doi.org/10.1111/j.1365-3040.2009.01934.x

Yin X, Belay D, van der Putten PL, Struik P (2014) Accounting for the decrease of photosystem photochemical efficiency with increasing irradiance to estimate quantum yield of leaf photosynthesis. Photosynth Res 122(3):323–335. https://doi.org/10.1007/s11120-014-0030-8

Zaks J, Amarnath K, Kramer DM, Niyogi KK, Fleming GR (2012) A kinetic model of rapidly reversible nonphotochemical quenching. Proc Natl Acad Sci 109(39):15757–15762. https://doi.org/10.1073/pnas.1211017109

Zhang N, Portis AR (1999) Mechanism of light regulation of Rubisco: a specific role for the larger Rubisco activase isoform involving reductive activation by thioredoxin-f. Proc Natl Acad Sci 96(16):9438–9443

Zhu X-G, de Sturler E, Long SP (2007) Optimizing the distribution of resources between enzymes of carbon metabolism can dramatically increase photosynthetic rate: a numerical simulation using an evolutionary algorithm. Plant Physiol 145(2):513–526. https://doi.org/10.1104/pp.107.103713

Zhu XG, Wang Y, Ort DR, Long SP (2013) e-photosynthesis: a comprehensive dynamic mechanistic model of C3 photosynthesis: from light capture to sucrose synthesis. Plant Cell Environ 36(9):1711–1727